Published in final edited form as:
Nat Immunol. 2018 December ; 19(12): 1341–1351. doi:10.1038/s41590-018-0237-5.

Myeloid-derived suppressor cells control B cell accumulation in the CNS during autoimmunity

Benjamin Knier[1,2], **Michael Hiltensperger**[1], **Christopher Sie**[1], **Lilian Aly**[1,2], **Gildas Lepennetier**[1,2], **Thomas Engleitner**[3,4], **Garima Garg**[1], **Andreas Muschaweckh**[1], **Meike Mitsdörffer**[1,2], **Uwe Koedel**[5], **Bastian Höchst**[6], **Percy Knolle**[6], **Matthias Gunzer**[7], **Bernhard Hemmer**[2,8], **Roland Rad**[3,4], **Doron Merkler**[9], and **Thomas Korn**[1,2,8,*]

[1]Department of Experimental Neuroimmunology, Klinikum rechts der Isar, Technical University of Munich, Munich, Germany [2]Department of Neurology, Klinikum rechts der Isar, Technical University of Munich, Munich, Germany [3]Institute of Molecular Oncology and Functional Genomics, TransaTUM Cancer Center, Technical University of Munich, Munich, Germany [4]Department of Medicine II, Klinikum rechts der Isar, Technical University of Munich, Munich, Germany [5]Department of Neurology, Klinikum Grosshadern, Ludwig Maximilians University Munich, Munich, Germany [6]Institute of Molecular Immunology and Experimental Oncology, Technical University of Munich, Munich, Germany [7]Institute for Experimental Immunology and Imaging, University Hospital Essen, University of Duisburg-Essen, Essen, Germany [8]Munich Cluster for Systems Neurology (SyNergy), Munich, Germany [9]Department of Pathology and Immunology, Division of Clinical Pathology, University of Geneva, Genève, Switzerland

Abstract

PMN-MDSCs (polymorphonuclear myeloid-derived suppressor cells) have been characterized in the context of malignancies. Here we found that PMN-MDSCs had the unique ability to restrain B cell accumulation during central nervous system (CNS) autoimmunity. $Ly6G^+$ cells were recruited to the CNS during experimental autoimmune encephalomyelitis (EAE), interacted with B cells that produced the cytokines GM-CSF and IL-6, and acquired properties of PMN-MDSCs in the CNS in a manner dependent on the signal transducer STAT3. Depletion of $Ly6G^+$ cells or dysfunction of $Ly6G^+$ cells through conditional ablation of STAT3 resulted in the selective

*Correspondence: Thomas Korn, Klinikum rechts der Isar, Technical University of Munich, Ismaninger Str. 22, 81675 Munich, Germany; Phone: ++49-89-41405617; Fax: ++49-89-41404675; thomas.korn@tum.de.

Data availability

The data that support the findings of this study are available from the corresponding author upon request.

Author contributions

BK conceptualized parts of the study, performed most of the experiments, analyzed data, and wrote the manuscript. MH, CS, LA, GG, AM, and MM performed experiments and analyzed data. GL, TE, and RR performed and analyzed the RNAseq experiments. UK developed CSF drainage technique and performed certain experiments. DM performed histology and analyzed data. BHö, PK, MG, and BH designed experiments and analyzed data. TK conceptualized and directed the study, supervised the experiments, analyzed data, and wrote the manuscript.

Competing financial interests: The authors declare no competing financial interests.

Accession codes: RNAseq data have been deposited in the Gene Expression Omnibus database under the accession code PRJEB28339.

Europe PMC Funders Author Manuscripts

Europe PMC Funders Author Manuscripts

accumulation of GM-CSF-producing B cells in the CNS compartment, which in turn promoted an activated microglial phenotype and failure to recover from EAE. The frequency of $CD138^+$ B cells in the cerebrospinal fluid (CSF) of human patients with multiple sclerosis negatively correlated with the frequency of PMN-MDSCs in the CSF. Thus, PMN-MDSCs might selectively control the accumulation and cytokine secretion of B cells within the inflamed CNS.

Suppressive myeloid cells were first described in tumor models accompanied by a strong leukemoid reaction 1. Based on surface markers in mice and humans, mononuclear (monocytic) myeloid-derived suppressor cells (M-MDSCs) and polymorphonuclear (granulocytic) MDSCs (PMN-MDSCs) have been described 2. The surface lectin-type receptor LOX1, encoded by the *OLR1* gene, was shown to be specifically expressed on PMN-MDSCs in humans 3. In mice, PMN-MDSCs are characterized as $CD11b^+Ly6G^+Ly6C^{int}$, which are also markers for *bona fide* neutrophils. However, because PMN-MDSCs are considered as aberrantly activated neutrophils, the imprinting of distinct signaling pathways in $CD11b^+Ly6G^+Ly6C^{int}$ cells can be used to detect MDSCs in tissues of mice and humans. For instance, PMN-MDSCs respond to signals transduced by the transcription factor STAT3 for expansion and survival *in situ* and robust activation of STAT3 is a hallmark of PMN-MDSCs and secures their functional phenotype 4. PMN-MDSCs strongly suppress $CD8^+$ T cell responses against tumor cells. Less is known about the role of PMN-MDSCs in autoimmunity. PMN-MDSCs have been shown to interact with B cells to inhibit the proliferation and differentiation of B cells *in vitro* 5 and *in vivo* 6, or to induce regulatory B cells 7 or IgA^+ antibody-secreting cells 8. PMN-MDSCs also prevent the expansion of $CD19^+CD138^+$ B cells in an indirect manner, by suppressing T follicular helper cell functions 9.

Despite the efficacy of B cell-depleting therapies in multiple sclerosis (MS), the function of B cells in MS is not well defined. B cells serve as precursors of antibody-secreting cells and provide cytokines, in particular IL-6, to promote germinal center reactions. B cells also present their cognate antigen to T cells and give T cell help. Compelling data supporting all of these functions have been reported in the context of central nervous system (CNS) autoimmunity in preclinical models 10,11. Circumstantial evidence from clinical trials suggests that B cell-depleting therapies in MS might mainly affect the antigen-presenting function of B cells 12. Notably, repopulating B cells after B cell depletion are skewed to produce IL-10 instead of GM-CSF and contribute to sustained tolerance 13. Thus, in addition to their function as antigen-presenting cells, B cells might also exert a damaging function due to the secretion of cytokines. Finally, there is an ongoing debate about the structure and function of aggregates of B cells in the subarachnoid space. In particular, the initiation and severity of the chronic disease phase in MS has been associated with the accumulation of these B cell aggregates 14. Therefore, B cells appear to facilitate a compartmentalized inflammatory process in the CNS that is disconnected from the systemic immune system.

Here, we sought to investigate the autoregulatory loops that control the recruitment, maintenance and function of B cells in the cerebrospinal fluid (CSF) and CNS parenchyma. $Foxp3^+$ regulatory T cells (T_{reg} cells) directly regulate some functions of B cells 15–17.

However, in experimental autoimmune encephalomyelitis (EAE), depletion of T_{reg} cells leads to an exacerbated disease course dependent on an enhanced effector T cell response, but independent of B cells 18, suggesting that Foxp3$^+$ T_{reg} cells dominantly regulate autoreactive T cells. Here we show that PMN-MDSCs inhibit the recruitment, local proliferation and cytokine secretion of CD138$^+$ B cells in the CSF space and CNS parenchyma. Ly6G$^+$ cells differentiated into PMN-MDSCs in the CNS in a gp130-STAT3-dependent manner.

Results

PMN-MDSCs inversely correlate with CD138$^+$ B cells in CSF

Plasmablasts in the CSF are associated with disease activity in neuroinflammatory disorders, including MS and neuromyelitis optica 19,20. We tested whether an inverse correlation between the CSF plasmablast fraction and the fraction of any other immune cell population would indicate a potential regulatory relationship. In the CSF of patients with a first clinical episode suggestive of MS (i. e. clinically isolated syndrome (CIS)) or established MS, we found a robust negative correlation between the frequency of CD19$^+$CD138$^+$ B cells and the frequency of CD15$^+$CD11b^{int}LOX1$^+$ myeloid cells (Fig. 1a), but not with the frequency of LOX1$^-$ myeloid cells, total polymorphonuclear cells (PMN) or any other immune cell subset in the CSF, including CD4$^+$ T cells, CD8$^+$ T cells, NK cells or CD14$^+$ monocytes (Fig. 1a, Supplementary Fig. 1). CD15$^+$CD11b^{int}LOX1$^+$ myeloid cells have been identified as PMN-MDSCs in humans 3. In contrast to granulocytes, PMN-MDSCs are found in the low-density fraction in dual density gradient purification of peripheral blood cells and have a "monocytic" appearance (Fig. 1b), which is in line with the fact that *bona fide* polymorphonuclear cells are not regularly found in CSF samples of MS patients. Upon co-culture *in vitro*, CD15$^+$CD11b^{int}LOX1$^+$ myeloid cells, but not LOX1$^-$ granulocytes, suppressed the proliferation of B cells stimulated with antibodies against CD40 and IL-4 (Fig. 1c), indicating that the negative correlation between the plasmablasts and PMN-MDSCs in the CSF of MS patients could be due to the suppressive activity of PMN-MDSCs towards B cells.

Next, we evaluated the suitability of PMN-MDSCs as a potential marker for reduced disease activity in CIS and MS patients. LOX1$^+$ PMN-MDSCs, but not M-MDSCs were increased in the peripheral blood of CIS and MS patients compared to healthy control subjects (Fig. 1d), suggesting that an inflammatory disease can trigger the appearance of PMN-MDSCs in the peripheral blood. Importantly, the frequency of LOX1$^+$ PMN-MDSCs was significantly lower in MS patients that had experienced a recent relapse compared to stable MS patients (Fig. 1e), a pattern that was observed irrespective of whether or not the patients were on disease-modifying therapy (Fig. 1f). Moreover, when analyzing paired blood samples of MS patients during relapse and at a follow-up visit (between 1 to 15 months later), the frequency of LOX1$^+$ PMN-MDSCs increased in the MS patients in whom inflammatory disease activity was entirely controlled and who were in a state known as "no evidence of disease activity" (NEDA-3), compared to patients with ongoing disease activity (Supplementary Fig. 1). Thus, PMN-MDSCs were detectable in chronic CNS autoimmunity and their frequency

in the peripheral blood was decreased during episodes of active inflammatory disease, suggesting that PMN-MDSCs might be involved in the regulation of disease activity in MS.

Ly6G$^+$ cells persist in the CSF of mice during recovery from EAE

To test the function of PMN-MDSCs in autoimmune neuroinflammation, we induced EAE in mice by immunization with myelin oligodendrocyte glycoprotein (MOG) peptide 35-55 in complete Freund's adjuvant (CFA), which reflects many immune-mediated aspects of human MS 21. We used Ly6G-tdTomato reporter mice, in which Ly6G$^+$ cells can be tracked by expression of tdTomato (hereafter *Ly6g*$^{Cre/WT}$) 22, and analyzed Ly6G-tdTomato$^+$ cells in the CNS, CSF and the blood during EAE. We observed an increase in the fraction of Ly6G-tdTomato$^+$ cells at disease onset (day 10-12) and a persisting population of Ly6G-tdTomato$^+$ cells during the recovery phase (day 20-22) in the CSF compared to blood (Fig. 2a, b), concomitant with a second "peak" of CXCL1 protein expression in the CSF (Fig. 2c). Phenotypically, the "monocytic" appearance of Ly6G-tdTomato$^+$ cells during the recovery phase was reminiscent of PMN-MDSCs, but very different from that of Ly6G-tdTomato$^+$ cells collected from the peripheral immune compartment, which had segmented nuclei (Fig. 2d). iNOS was highly expressed and arginase activity strongly increased in Ly6G-tdTomato$^+$ cells isolated from the CNS at recovery as compared to onset (Fig. 2e, f). Taken together, these data suggested that the Ly6G-tdTomato$^+$ cells in the CNS during the recovery phase were phenotypically similar to PMN-MDSCs.

Ly6G$^+$ cells acquire an MDSC-like transcriptome in the CNS

To obtain a more comprehensive understanding of PMN-MDSCs during CNS autoimmunity, we performed RNA-seq analysis on Ly6G-tdTomato$^+$ cells sorted from the spleen and CNS of *Ly6g*$^{Cre/WT}$ mice at onset (day 12) and during the recovery phase (day 22) of EAE. Principal component analysis segregated CNS-derived Ly6G-tdTomato$^+$ cells from spleen-derived Ly6G-tdTomato$^+$ cells (Fig. 3a). In particular, the transcriptome of CNS-derived Ly6G-tdTomato$^+$ cells at onset appeared to be most distinct from all other subsets according to PC1, and two MDSC hallmark genes, *Nos2* and *Arg1*, were significantly upregulated in CNS onset, but not CNS recovery Ly6G-tdTomato$^+$ cells compared to their expression in spleen Ly6G-tdTomato$^+$ cells (Supplementary Fig. 2). Because Nos2 and Arg1 protein were highly upregulated in CNS recovery Ly6G-tdTomato$^+$ cells compared to CNS onset Ly6G-tdTomato$^+$ cells (Fig. 2e, f), these data suggested that the transcriptome of CNS onset Ly6G-tdTomato$^+$ cells reflected the functional phenotype of CNS recovery Ly6G-tdTomato$^+$ cells, consistent with the delay imparted by RNA translation into protein. Moreover, in gene set enrichment analyses, a set of known human MDSC signature genes (such as *PRDX1*, *OLR1*, *IRF8*, *DOCK10*) 3 was enriched in samples with high PC1 and PC3 ranks (Fig. 3b, Supplementary Fig. 2), indicating that the transcriptome of CNS onset Ly6G-tdTomato$^+$ cells was the most similar with a PMN-MDSC profile.

To further analyze the transcriptome of CNS onset Ly6G-tdTomato$^+$ cells we identified 484 genes as universally downregulated and 1,110 genes as universally upregulated in CNS onset Ly6G-tdTomato$^+$ cells compared to all other Ly6G-tdTomato$^+$ cell subsets, respectively (Supplementary Table 1). Among the genes differentially downregulated in CNS onset Ly6G-tdTomato$^+$ cells, gene ontology terms including oxidoreductase activity, co-enzyme

binding, and histone kinase activity were significantly overrepresented, while cytokine receptor binding, amide binding, and enzyme inhibitor activity were significantly enriched within the set of genes universally upregulated in CNS onset Ly6G-tdTomato$^+$ cells (Fig. 3c, Supplementary Fig. 2, Supplementary Tables 2 and 3). Notably, the mRNA for *Olr1*, the mouse homologue of human *OLR1* (which encodes LOX1), was significantly upregulated in CNS onset Ly6G-tdTomato$^+$ cells compared to all other Ly6G-tdTomato$^+$ populations (Supplementary Table 1). In summary, the PMN-MDSC signature was restricted to CNS Ly6G-tdTomato$^+$ cells, while splenic Ly6G-tdTomato$^+$ cells did not show an MDSC-like profile.

To test whether Ly6G$^+$ cells acquired the MDSC profile within the inflamed CNS compartment we transferred Ly6G-tdTomato$^+$ cells isolated from the spleen of MOG(35-55) plus CFA-immunized CD45.2$^+$ *Ly6g*$^{Cre/WT}$ mice into MOG(35-55) plus CFA-immunized congenic CD45.1$^+$ host mice two days after onset of clinical signs of EAE and tracked CD45.2$^+$Ly6G-tdTomato$^+$ cells at days 1, 4, and 7 after transfer in the spleen and the CNS of host animals. While transferred CD45.2$^+$Ly6G-tdTomato$^+$ cells disappeared from the peripheral immune compartment within two days, they accumulated and persisted within the CNS (Fig. 3d, e). Donor CD45.2$^+$Ly6G-tdTomato$^+$ cells were Ki67 positive in the inflamed host CNS, but not in the spleen and CNS-derived Ly6G-tdTomato$^+$ cells expressed high amounts of iNOS compared to Ly6G-tdTomato$^+$ cells re-isolated from the spleen (Fig. 3f). These data indicated that Ly6G-tdTomato$^+$ cells converted into PMN-MDSCs and accumulated within the CNS compartment.

Ly6G$^+$ MDSCs prevent the perpetuation of clinical signs of EAE

Given the overlap in phenotype between human PMN-MDSCs and murine Ly6G-tdTomato$^+$ cells isolated from the CNS parenchyma, we tested whether the ablation or genetic loss of function of these cells in mice affected EAE progression. First, we depleted MDSCs in *Ly6g*$^{Cre/WT}$ mice with a monoclonal antibody directed against Ly6G starting at day 12, after onset of EAE. The depletion efficiency was around 90% in the blood and 80% in the CNS, as monitored by Ly6G-tdTomato expression (Supplementary Fig. 3). In contrast to control antibody-treated mice, Ly6G-tdTomato$^+$ MDSC-depleted *Ly6g*$^{Cre/WT}$ mice failed to recover from clinical signs of disease (Fig. 4a). Conversely, expansion of Ly6G$^+$ cells by administration of G-CSF as of day 12, resulted in faster and more complete recovery from clinical disease as compared to control-treated mice (Fig. 4b), suggesting that Ly6G$^+$ cells were suppressive as of the peak of EAE (after day 16).

The numbers of CD11b$^+$CD45^{hi} macrophages and CD4$^+$ T cells as well as the fraction of IL-17-, IFN-γ-, GM-CSF-, and IL-10-producing CD4$^+$ T cells and Foxp3$^+$ T_{reg} cells recovered from the CNS on day 21 were similar in control antibody-treated and Ly6G-tdTomato$^+$ MDSC-depleted *Ly6g*$^{Cre/WT}$ mice (Supplementary Fig. 4). However, we detected a significant (about 3-fold) increase in the frequency and total number of CD19$^+$ B cells in the spinal cord of Ly6G-tdTomato$^+$ MDSC-depleted *Ly6g*$^{Cre/WT}$ mice as compared to control antibody-treated mice (Fig. 4c, e), and a reduction in the frequency and number of CD19$^+$ B cells in the spinal cord of mice treated with G-CSF as compared with vehicle (5% glucose)-treated *Ly6g*$^{Cre/WT}$ mice (Fig. 4d, f). The frequencies of CD19$^+$ B cells inversely

correlated with the frequencies of Ly6G$^+$ cells in the CNS parenchyma of G-CSF-treated and control-treated *Ly6g*$^{Cre/WT}$ mice at early disease recovery (day 21) (Fig. 4g). In addition, Ly6G-tdTomato$^+$ cells isolated from the CNS of *Ly6g*$^{Cre/WT}$ mice at early recovery (day 20) suppressed the proliferation of B cells stimulated with antibodies against CD40 and IL-4 following *in vitro* co-culture compared to Ly6G-tdTomato$^+$ cells isolated from the CNS of *Ly6g*$^{Cre/WT}$ mice at day 12 (EAE-onset) and Ly6G-tdTomato$^+$ cells isolated from the spleen of *Ly6g*$^{Cre/WT}$ mice at all disease stages, which did not suppress the proliferation of B cells in co-cultures (Fig. 4h). These data suggested that Ly6G-tdTomato$^+$ cells modulated inflammation during EAE by inhibiting the proliferation of B cells in the CNS.

STAT3 mediates Ly6G$^+$ cell conversion into MDSCs in the CNS

Myeloid bone marrow precursors generate PMN-MDSCs following stimulation with GM-CSF and IL-6 in a manner dependent on C/EBPβ 23. Based on qPCR, gp130 (encoded by *Il6st*), the signaling subunit of the IL-6 receptor complex was among the top genes upregulated in CNS-derived Ly6G-tdTomato$^+$ cells compared to splenic Ly6G-tdTomato$^+$ cells (Fig. 5a). RNA-seq on Ly6G-tdTomato$^+$ cells indicated that STAT3-targeted genes 24 were highly enriched in CNS onset Ly6G-tdTomato$^+$ cells compared to CNS recovery and spleen Ly6G-tdTomato$^+$ cells (Fig. 5b). To test whether STAT3-dependent signaling determined the functional phenotype of Ly6G-tdTomato$^+$ cells in the CNS we generated mice with a conditional deletion of STAT3 in Ly6G$^+$ cells (*Stat3*$^{\Delta Ly6G}$ hereafter) by crossing *Ly6g*$^{Cre/WT}$ with *Stat3*$^{flox/flox}$ mice. *Stat3*$^{\Delta Ly6G}$ mice developed more severe EAE and did not recover from EAE as of day 20 (Fig. 5c), similar to Ly6G-tdTomato$^+$ MDSC-depleted mice. Conditional deletion of gp130 in *Ly6g*$^{Cre/WT}$ mice recapitulated the phenotype of *Stat3*$^{\Delta Ly6G}$ mice (Supplementary Fig. 5), while deletion of *Il6ra*, the IL-6 binding α-subunit of the IL-6 receptor complex, in Ly6G$^+$ cells in *Ly6g*$^{Cre/WT}$ x *Il6ra*$^{flox/flox}$ mice did not result in more severe EAE as compared to *Ly6g*$^{Cre/WT}$ control mice. These data suggested that the differentiation of PMN-MDSCs from Ly6G$^+$ precursors in the CNS was dependent on gp130 and STAT3.

In addition to the prolonged clinical phenotype in *Stat3*$^{\Delta Ly6G}$ mice, we observed an increase in the frequency of CD19$^+$ B cells in the CNS of *Stat3*$^{\Delta Ly6G}$ mice compared to *Ly6g*$^{Cre/WT}$ control mice (Fig. 5d). The number and phenotype of T cells as well as the number of monocytes in the CNS of *Stat3*$^{\Delta Ly6G}$ mice were similar to those observed in *Ly6g*$^{Cre/WT}$ controls (Supplementary Fig. 6), suggesting that the STAT3-dependent activation of Ly6G$^+$ MDSCs inhibited the accumulation of B cells but not other immune cells in the CNS during EAE. To address whether Ly6G$^+$ MDSCs inhibited B cell recruitment or B cell expansion in the CNS, we measured the concentration of CSF chemokines required for B cell recruitment to the CNS by cytometric bead array. The amount of CXCL1 and CXCL13 protein in the CSF was higher in the CSF of *Stat3*$^{\Delta Ly6G}$ mice than in *Ly6g*$^{Cre/WT}$ control mice on day 24 (Fig. 5e), suggesting that increased recruitment might explain part of the increase in CD19$^+$ B cells in the CNS of mice with STAT3-deficient Ly6G$^+$ cells. Ly6G$^+$ MDSCs suppress the proliferation of lymphocytes by a variety of mechanisms 25,26. Co-culture of Ly6G-tdTomato$^+$ MDSCs isolated from the CNS of wild-type mice during EAE recovery (day 21) with naive B cells that were stimulated with antibodies against CD40 plus IL-4 significantly suppressed B cell proliferation, while Ly6G-tdTomato$^+$ cells isolated from the CNS of

Stat3$^{\Delta Ly6G}$ mice did not (Fig. 5f). The inhibitory effect of wild-type Ly6G-tdTomato^{+} cells was blocked by the NOS inhibitor L-NMMA and by neutralizing antibodies to VISTA and to PD-L1 (CD274) (Fig. 5f). Ki67 staining *ex vivo* indicated an increase in Ki67 binding to B cells, but not to T cells isolated from the CNS of *Stat3*$^{\Delta Ly6G}$ mice as compared to their counterparts isolated from *Ly6g*$^{Cre/WT}$ control mice on day 21 (Fig. 5g). B cells rarely infiltrate the CNS of wild-type mice in MOG(35-55)-induced EAE (Fig. 5h). However, in immune histochemical analysis, there was a marked increase in the B cell numbers in *Stat3*$^{\Delta Ly6G}$ mice with MOG(35-55)-induced EAE compared to *Ly6g*$^{Cre/WT}$ controls after the peak of disease (day 23) (Fig. 5i). In addition to a few cells scattered in the parenchyma, the majority of CD19^{+}B220^{+} B cells in *Stat3*$^{\Delta Ly6G}$ mice were clustered together in the meninges (Fig. 5i, Supplementary Fig. 7). Together, these data suggested that Ly6G^{+} MDSCs suppressed B cell recruitment and proliferation in the meningeal compartment in wild-type mice during EAE.

Ly6G^{+} cells interact with B cells in the CNS

Next, we characterized B cells in the CNS in the presence or absence of Ly6G-tdTomato^{+} cells. The B cells in the CNS of *Stat3*$^{\Delta Ly6G}$ mice or in Ly6G-tdTomato^{+} MDSC-depleted *Ly6g*$^{Cre/WT}$ mice with EAE were IgM^{+}CD21^{-}CD35^{-} B cells. We observed a 30 % increase in activated CD23^{+} B cells in these mice as compared to wild-type EAE mice (Fig. 6a, Supplementary Fig. 7). There was no increase in the percentage of CD138^{+} plasma cells in either the spleen or the CNS of *Stat3*$^{\Delta Ly6G}$ mice compared to *Ly6g*$^{Cre/WT}$ controls (Fig. 6b). CD23 is an activation marker of B cells and CD23^{+} B cells in the CNS co-expressed IL-6 and GM-CSF (Fig. 6c). Neither CD1^{+}CD5^{+} B cells, which were reported to have regulatory properties 27 nor unconventional B1 cells, which are CD23^{low} 28, contributed to the increased numbers of B cells in the CNS of *Stat3*$^{\Delta Ly6G}$ mice or Ly6G-tdTomato^{+} MDSC-depleted *Ly6g*$^{Cre/WT}$ mice (Supplementary Fig. 7). A larger fraction of B cells in the brain and spinal cord of *Stat3*$^{\Delta Ly6G}$ mice than *Ly6g*$^{Cre/WT}$ control mice secreted GM-CSF, but not IL-10 on day 23 (Fig. 6d, e, Supplementary Fig. 7), consistent with a higher fraction of activated CD23^{+}IgM^{+} B cells in *Stat3*$^{\Delta Ly6G}$ mice as compared to *Ly6g*$^{Cre/WT}$ mice.

Most Ly6G-tdTomato^{+} cells in the CNS co-stained for phosphorylated STAT3 (pSTAT3) in immunohistochemical analyses (Fig. 6f), indicating the activation of this pathway in Ly6G^{+} cells in the inflamed CNS. Ly6G-tdTomato^{+} cells in the CNS of *Stat3*$^{\Delta Ly6G}$ mice did not express STAT3 (Fig. 6g). Notably, Ly6G-tdTomato^{+} cells were detected in close proximity to B220^{+} B cell aggregates in the meninges and superficial CNS parenchyma in *Stat3*$^{\Delta Ly6G}$ mice compared to *Ly6g*$^{Cre/WT}$ mice, which essentially lacked meningeal B cell infiltrates (Fig. 6f, h), suggesting a direct interaction between B cells and Ly6G^{+} cells in the meningeal compartment. To test whether direct interaction between B cells and Ly6G^{+} cells led to activation of STAT3 in Ly6G^{+} cells, splenic Ly6G^{+} cells from C57BL/6 mice immunized with MOG(35-55)+CFA were isolated on day 8 and incubated with IL-6 or a complex composed of soluble IL-6Rα and IL-6 (IL-6-IL-6Rα hereafter), which signals into cells even though they lack membrane IL-6Rα expression. STAT3 activation, as assessed by expression of pSTAT3, was higher in Ly6G^{+} cells in response to IL-6-IL-6Rα than in response to equimolar amounts of IL-6 (Fig. 6i), consistent with the reduced expression of IL-6Rα on the cell membrane of activated Ly6G^{+} cells. Notably, when Ly6G^{+} cells isolated

from the spleen of MOG(35-55)+CFA-immunized wild-type mice on day 8 were co-cultured with MOG B cell receptor transgenic CD19^{+} B cells isolated from the spleen of TH mice 29 that were activated to produce IL-6 *in vitro* by co-culture with MOG T cell receptor transgenic T cells 30 and MOG protein, we detected an increase in pSTAT3 only in Ly6G^{+} cells in direct contact with the B cells, but not in Ly6G^{+} cells separated from the B cells in a transwell chamber (Fig. 6j). The increase in pSTAT3 in Ly6G^{+} cells was partly reversible by blockade of IL-6Rα with a neutralizing antibody against IL-6Rα (Fig. 6j). These data suggested that direct cell contact between Ly6G^{+} cells and B cells was required to activate STAT3 in Ly6G^{+} cells and that such interactions in the CNS might drive the conversion of Ly6G^{+} cells into MDSCs, which in turn controlled the activation of B cells in the CNS.

B cells in the CNS prevent recovery from EAE in *Stat3*$^{\Delta Ly6G}$ mice

To test whether the diminished capacity to recover from EAE of *Stat3*$^{\Delta Ly6G}$ mice was due to the higher frequency of activated CD23^{+}IgM^{+} B cells in the CNS of these mice compared to *Ly6g*$^{Cre/WT}$ mice, we depleted the B cells by i.v. administration of an antibody to CD20. I.v. treatment with an antibody to CD20 every 5 days after EAE onset (day 12) resulted in significant depletion of B cells in the brain and spinal cord of *Stat3*$^{\Delta Ly6G}$ mice to numbers below those observed in wild-type EAE mice (Fig. 7a). In addition, the percentage of GM-CSF^{+} B cells in CD20 antibody-treated EAE *Stat3*$^{\Delta Ly6G}$ mice was similar to that found in wild-type EAE mice (Fig. 7b). Treatment with CD20 antibody exacerbated the clinical score of MOG(35-55)-induced EAE in wild-type mice compared to control antibody-treated wild-type mice (Fig. 7c), consistent with previous reports 31. In contrast, administration of the CD20 antibodies ameliorated clinical disease severity in MOG(35-55)-induced EAE in *Stat3*$^{\Delta Ly6G}$ mice as compared to control antibody-treated *Stat3*$^{\Delta Ly6G}$ mice (Fig. 7d), indicating that B cells are responsible for the exacerbated EAE and chronic disease phenotype in the *Stat3*$^{\Delta Ly6G}$ mice.

Activated microglia have been associated with chronic inflammation in the CNS. RNA-seq data from microglia isolated from a chronic EAE model, as well as from experimental models of amyotrophic lateral sclerosis and Alzheimer's disease have been used to define a "neurotoxic" microglia profile 32. As such, we tested whether dysfunction or depletion of MDSCs in the CNS of *Stat3*$^{\Delta Ly6G}$ mice or Ly6G-depleted mice impacted the phenotype of microglia. Because the TREM2-APOE pathway is upregulated in "neurotoxic" microglia 32, we tested the expression of candidate genes of the TREM2-APOE pathway in microglia from *Stat3*$^{\Delta Ly6G}$ mice and *Ly6g*$^{Cre/WT}$ control mice in late stages of EAE (day 22). As compared to *Ly6g*$^{Cre/WT}$ EAE mice, sorted microglia from *Stat3*$^{\Delta Ly6G}$ EAE mice showed significantly higher expression of *Clec7a*, *Gpnmb*, *Trem2* and *ApoE* (Supplementary Fig. 8) and lower expression of markers of homeostatic microglia, including *Tmem119*, *P2ry12* and *Sall1* at late stages of EAE (day 22) (Supplementary Fig. 8). Thus, dysfunctional Ly6G-tdTomato^{+} cells in the CNS of *Stat3*$^{\Delta Ly6G}$ mice promoted a neurotoxic microglia profile. Together, these data established an association of enhanced GM-CSF responses in B cells in the absence of functional MDSCs in the CNS with tissue destructive microglia activation.

Discussion

Here we show that immune regulatory PMN-MDSCs are found as LOX1$^+$ MDSCs in the CSF of MS patients and as Ly6G$^+$ MDSCs in the CNS of mice with EAE during the recovery stage. Our analyses indicate that Ly6G$^+$ neutrophils differentiate into MDSCs within the CNS of wild-type mice in a STAT3-dependent manner and in turn control the accumulation and activation of B cells in this compartment. Loss of MDSCs leads to activation of B cell in the CNS, which – in part by secretion of GM-CSF – contribute to the establishment of compartmentalized inflammation in the CNS. B cells might be inducing an MDSC phenotype in a subset of neutrophils in the CNS, establishing a negative feedback-loop that prevents perpetuation of inflammation within the CNS.

Bona fide neutrophils are short-lived. Their half-life is in the range of 5-10 h in the systemic compartment, and they must be constantly replenished by the bone marrow 33. Even though genetic tools for the study of neutrophils have been lacking, their role in EAE has been addressed 34 and they are considered to exert a proinflammatory function either by licensing endothelial cells at the blood-brain-barrier for the enhanced recruitment of inflammatory cells 35, by inducing the maturation of antigen-presenting cells in the CNS 36, or through direct tissue destruction 37. However, because the autoimmune attacks of the CNS in humans are rarely hyperacute, the proinflammatory role of neutrophils might be limited. Rather, myeloid cells of neutrophil origin that reside in parenchymal tissues for up to 6 days 38 may be more relevant for the disease course of CNS autoimmunity.

Analyses of immune cell population dynamics in the CSF and CNS parenchyma of mice during EAE revealed a persistent population of Ly6G$^+$ cells at the beginning of the recovery stage. Because CXCL1 was also upregulated in the CSF at this stage, it is likely that various chemokine cues attract Ly6G$^+$ precursors into the CSF space through CXCR2 expressed on Ly6G$^+$ cells 39. Murine CXCL1 is the functional homologue of the human CXCL1 and CXCL8, which are detected in the CSF of MS patients 40, and CXCL1 has been described as a hallmark effector molecule of T_H17 cell-driven autoimmunity in the CNS during EAE 41. Ly6G$^+$ cells recruited to the CSF space during EAE differentiated into MDSCs in a STAT3-dependent manner. Interestingly, hyperactivation of STAT3 in LysM$^+$ cells, which also comprise a subset of neutrophils, results in expansion of MDSCs in the colon and protection from experimental colitis 42. While the differentiation of Ly6G$^+$ cells into MDSCs in the CNS required gp130 and STAT3, it remains to be determined which ligands are responsible for this process. The significance of IL-6 in expanding and activating MDSCs has been reported previously 43, and we confirmed that steady-state neutrophils express IL-6Rα, the IL-6-binding subunit of the IL-6R. However, once activated, neutrophils shed the IL-6Rα and most CNS Ly6G$^+$ cells lack IL-6Rα expression in EAE, consistent with the lack of a clinical phenotype in *Il6ra*$^{\Delta Ly6G}$ mice. Nevertheless, because cells lacking IL-6Rα expression are still able to receive IL-6 signals through IL-6 trans-signaling or IL-6 trans-presentation 44, it is possible that the local differentiation of Ly6G$^+$ cells into MDSCs occurs through cells that have the potential to present IL-6 in *trans*. Because B220$^+$ B cells were located in close proximity with Ly6G$^+$ cells in the meningeal space of *Stat3*$^{\Delta Ly6G}$ mice, it is intriguing to speculate that B cells, which produce IL-6 and can present it in *trans* through their own IL-6Rα, induce Ly6G$^+$ cells differentiation into MDSCs, which in turn

would suppress B cells activation. Consistent with this idea, antigen-stimulated IL-6^{+} B cells activated STAT3 in Ly6G^{+} cells only when the cells were in direct physical contact. Their residence in the same anatomical compartment, i. e. the meningeal space and superficial CNS parenchyma in the inflamed CNS, might explain the preferential suppression of B cell accumulation by Ly6G^{+} MDSCs while *ex vivo* Ly6G^{+} MDSCs from the CNS express both B cells and T cells 45.

MOG(35-55)-induced EAE in wild-type C57BL/6 mice is a model of T cell-mediated autoimmunity in the CNS, which is *per se* independent of B cells 46. There are no B cells in the CNS in this model 47. B cells might even have a regulatory function in the spleen in MOG(35-55)-induced EAE, possibly by secretion of IL-10 or IL-35 48,49. Depletion of B cells in this model results in a more severe disease31. Conversely, in EAE models in which B cells serve as antigen presenting cells, as sources of inflammatory cytokines or as precursors of cells that secrete pathogenic antibodies, depletion of B cells ameliorates the severity of EAE 31,50. Our data suggest that MDSCs in the CNS prevent the accumulation of B cells in the meningeal space and CNS parenchyma. When released from MDSC-mediated suppression, B cells accumulate within the CNS compartment even in MOG(35-55)-induced EAE, and through their secretion of inflammatory cytokines – in particular GM-CSF – promote immunopathology. GM-CSF production has been reported in the so-called innate responses activator (IRA) B cells, which are thought to be derived from peritoneal B1 cells in a MyD88-dependent manner upon TLR4 stimulation 28. The GM-CSF $^{+}$ B cells the CNS compartment of *Stat3*$^{\Delta Ly6G}$ mice were CD43^{+}CD93^{+}, similar to the IRA B cells; however, they were CD23^{+} and produced IL-6, suggesting they were more likely derived from conventional B cells. We did not observe an increase in plasma cells in the CNS of *Stat3*$^{\Delta Ly6G}$ mice. Yet, a potential impact of MDSCs on germinal center reactions in the CNS needs further investigation.

In conclusion, our study describes an interaction between PMN-MDSCs and a subset of IL-6 and GM-CSF-producing B cells in CNS autoimmunity. These two immune cell subsets are linked in a negative feedback-loop. Therapeutic interventions modulating this interaction might hold the potential to prevent the perpetuation of inflammatory responses in the CNS compartment in chronic autoimmune diseases where local aggregates of B cells are drivers of immunopathology.

Online Methods

Patients

Patients with diagnosis of relapsing remitting MS or CIS between 18 and 60 years of age were recruited from our department between 2017 and 2018. Relapsing remitting MS was defined using the 2010 McDonald criteria 51. Patients underwent lumbar puncture with CSF analysis for diagnostic work-up of suspected demyelinating inflammatory disease of the CNS before initiation of any immunomodulatory treatment. PBMCs were collected from MS/CIS patients under disease-modifying therapies with IFN-β1a/b, glatiramer acetate, dimethyl fumarate, teriflunomide, natalizumab, fingolimod, ocrelizumab, or without any disease-modifying therapy. The study was approved by the local ethics committee (Ethics

commission, TUM Medical School, Technical University of Munich) and conducted following the Declaration of Helsinki. All patients provided written informed consent.

Preparation of human PBMCs, flow cytometric analysis of PMBC and CSF cells

PBMCs were isolated using Ficoll density gradient centrifugation (1.077 g/ml, Merck, Darmstadt, Germany). Both CSF and PBMC samples were immediately processed after collection. Albumin, IgG, IgM, and IgA were measured in cell free CSF and serum using a BNProSpec (Siemens, Erlangen, Germany) analyzer. For cytometry, fresh CSF cells or freshly prepared PBMCs were washed with 2% fetal calf serum/phosphate-buffered saline and surface stained using anti-human CD3 (UCHT1), CD4 (RPA_T4), CD8 (SK1), CD11b (ICRF44), CD14 (M5E2), CD15 (HI98), CD19 (HIB19), CD33 (P67.6), CD45 (HI30), CD56 (N901), CD138 (MI15), HLA-DR (L243) and anti-human LOX1 (15C4), which were purchased from either Biolegend, eBioscience or BD Biosciences.

Mice

Congenic CD45.1 mice 52 and *Il6st*$^{flox/flox}$ (*Il6st*^{tm1Wme}) mice 53 were obtained from Jackson Laboratory. *Ly6g*$^{Cre/WT}$ mice were generated as previously described 22, *Stat3*$^{flox/flox}$ (*Stat3*^{tm2Aki}) mice 54 were a gift of F. Greten (Institute for Tumor Biology and Experimental Therapy, Georg-Speyer Haus, Frankfurt, Germany) and *Il6ra*$^{flox/flox}$ mice 55 were a gift of T. Wunderlich (Max-Planck-Institute for Metabolism Research, Cologne, Germany). To generate mice with cell type-specific excision of *lox*P-flanked cassettes, mice with *lox*P-flanked alleles were bred with *Ly6g*$^{Cre/WT}$ mice. All mouse strains were on pure C57BL/6 background. Animals were kept in a specific pathogen-free facility at the University of Essen and the Technical University of Munich. All experimental protocols were approved by the standing committee for experimentation with laboratory animals of the administration of Upper Bavaria (AZ 55.2-1-54-2532-95-2014, AZ 55.2-1-54-2532-29-13, AZ ROB-55.2-2532.Vet_02-17-69, AZ ROB-55.2-2532.Vet_03-18-53) and performed in accordance with the corresponding guidelines.

Induction of EAE, cell depletion, drainage of murine cerebrospinal fluid

EAE was induced by subcutaneous application of an emulsion containing 200 μg MOG(35-55) peptide (MEVGWYRSPFSRVVHLYRNGK) and 500 μg *Mycobacterium tuberculosis* H37Ra (Difco, Detroit, USA) in Freund's adjuvant oil plus intravenous (i.v.) injection of 200 ng pertussis toxin (Sigma-Aldrich, St. Louis, USA) on days 0 and 2. Mice were rated blinded on a score from 0 to 5 (0 = no disease signs; 1 = tail paresis; 2 = unsteady gait; 3 = paraplegia; 4 = tetraplegia; 5 = death). Mice typically reached disease onset between days 10-12 after immunization, suffered from peak disease between days 15-18 and started to recover at day 20-22 after immunization. Ly6G^{+} neutrophils were depleted by intraperitoneal (i.p.) application of 400 μg anti-Ly6G antibody every other day (clone 1A8; Bio X Cell, West Lebanon, USA). Rat IgG2a served as control (clone 2A3; Bio X Cell). B cells were depleted by i.v. administration of 10 μg/g anti-CD20 antibody every 5 days (clone 18B12, courtesy from the Monoclonal Antibody Core Facility & Research Group, Helmholtz Zentrum Munich, Germany). Mouse IgG1 (clone MOPC-21, Bio X Cell) served as control. For CSF collection, mice were anesthetized with buprenorphine, ketamine, xylazine, and CSF was aspirated from the cisterna magna after burr hole trepanation. Mice

Europe PMC Funders Author Manuscripts

underwent intravascular staining procedure 56 with 3 μg of pacific blue labeled anti-CD45.2 antibody (clone 104, Biolegend, San Diego, USA) in 300 μl PBS i.v. 3 minutes before trepanation to discriminate CSF from artificial blood leukocytes. Only macroscopically bloodless CSF samples were used for further analysis. CSF samples underwent centrifugation. Clear supernatants were frozen at -80°C for further analysis (see below), CSF cell pellets underwent further analysis by cytometry (see below) immediately. Mice were sacrificed after CSF drainage.

Preparation of mononuclear cells

Mice were anesthetized with isoflurane or with buprenorphine, ketamine and xylazine. After perfusion through the left cardiac ventricle with cold PBS, brain and spleen were dissected; the spinal cord was flushed out of the spinal canal with PBS by hydrostatic pressure. The spinal cord was dissected from the brain at the level of the medulla oblongata, optic nerves were dissected stereo-microscopically between the optic disc and the optic chiasm. CNS tissues were digested separately with 1.0 mg/ml collagenase d (Roche, Basel, Switzerland) and 40 μg/ml DNaseI (Sigma-Aldrich) at 37°C for 45 minutes. CNS cells were isolated by passing the tissue through a 70 μm cell strainer and by 37% Percoll gradient centrifugation. Splenic tissue was passed through a 70 μm cell strainer, erythrocyte lysis was performed afterwards. The cell pellet was washed and resuspended in culture medium for further analysis.

Antibodies, flow cytometry and sorting

Cell suspensions were treated with Fc block CD16/CD32 (2.4G2) and surface markers were stained with fluorochrome conjugated anti-mouse CD3 (145-2C11), CD4 (RM4-5), CD11b (M1/70), CD19 (1D3), CD23 (B3B4), CD43 (S11), CD45R/B220 (RA3-6B2), CD45.1 (A20), CD45.2 (104), CD93 (AA4.1), CD138 (281-2), IgM (RMM-1), Ly6G (1A8), MHC-II (M5/114.15.2). For dead cell exclusion, LIVE/DEAD® fixable Near-IR stain kit (Invitrogen, Carlsbad, USA) was used. For intracellular staining, Foxp3 staining kit (eBioscience, Thermo Fisher, Waltham, USA) was used for Foxp3 (FKJ-16s), GM-CSF (MP1-22E9), IL-6 (MP5-20F3), IL-10 (JES5-16E3), IL-17 (TC11-18H10), IFN-γ (XMG1.2), Ki67 (16A8) and NOS2 (CXNFT). All antibodies were purchased from either Biolegend, eBioscience or BD Biosciences (Franklin Lakes, USA). For intracellular cytokine staining, cells were stimulated in culture medium containing phorbol 12-myristate 13-acetate (PMA, 20 ng/ml, Sigma-Aldrich), ionomycin (1 μg/ml, Sigma-Aldrich), and monensin (GolgiStop 1 μl/ml, BD Biosciences) at 37 °C/5% CO_2 for 2 h. Flow cytometric analysis was performed on a CyAn ADP or CytoFLEX flow cytometer (Beckman Coulter, Brea, USA) or a FACS Aria III (BD Biosciences), and flow cytometric data were analyzed using FlowJo software (Tree Star, Ashland, USA). FACS sorting was performed on a FACS Aria III (BD Biosciences).

Analysis of cytokine and chemokine levels in murine CSF

Frozen CSF samples were cautiously thawed. Cytokine and chemokine levels were measured in 5 μl CSF using a bead-based immunoassay according to the manufacturer's instructions (LEGENDplex, Biolegend). Analysis was down using a CytoFLEX flow cytometer (Beckman Coulter).

B cell proliferation suppression assay

For murine B cell proliferation assays, responder $CD19^+B220^+$ B cells were highly purified by FACS sorting from naïve spleens of *Ly6g*$^{Cre/WT}$ mice and plated in 96-well U bottom plates. In each well, 2,000 or 5,000 B cells were stimulated in culture medium containing 5% fetal calf serum with 50 μg/ml anti-CD40 (FGK4.5, Bio X Cell) and 10 ng/ml IL-4 (Milteny Biotec, Bergisch Gladbach, Germany) at 37°C and 5% CO_2 for 72 hours and were co-cultured with $Ly6G^+$ suppressor cells in different ratios. To test blocking of suppression, 0.5 mM N-monomethyl-L-arginine (L-NMMA, NOS2 inhibitor, Sigma-Aldrich), 0.5 mM N-hydroxy-L-arginine (L-NOHA, Arginase 1 inhibitor, Sigma-Aldrich), 5 μg/ml anti-CD274 (anti-PD-L1, 10F.9G2, Biolegend), or 5 μg/ml anti-VISTA (MH5A, Biolegend) were added. For human B cell proliferation assays, responder $CD19^+CD27^-$ responder B cells and $CD15^+CD11b^{int}$ $CD33^{high}LOX1^{high}$ MDSCs were purified from PBMC samples of the same individual and plated in U bottom plates. $CD15^+CD11b^{high}CD33^{low}LOX1^{low}$ neutrophils purified from whole blood samples of the same individuals after erythrocyte lysis served as controls. In each well, 8,000 B cells were stimulated with 1 μg/ml anti-CD40 (G28.5, Bio X Cell) and 20 ng/ml IL-4 (Miltenyi Biotec) at 37°C and 5% CO_2 for 72 hours and were co-cultured with MDSCs or neutrophils in different ratios. After 57 hours, all wells were pulsed with 1 mCi H^3-thymidine and harvested 15 hours later for assessment of thymidine incorporation by scintillation counting (PerkinElmer, Waltham, USA). All conditions were run as triplicates.

Transwell *in vitro* culture

TCR transgenic MOG-specific $CD4^+$ T cells and BCR transgenic MOG-specific $CD19^+$ B cells were FACS-purified from naïve 2D2 mice 30 and TH mice 29, respectively. 100,000 T and 100,000 B cells per well were stimulated with 5 μg/ml recombinant rat MOG Protein (1-125) (Biotrend, Cologne, Germany) for 48h. Splenic $Ly6G^+CD11b^+$ cells were FACS-purified from wild type mice on d7 after immunization with CFA, and 125,000 $Ly6G^+CD11b^+$ cells were then added to the T-B coculture into the bottom compartment of a transwell system (HTS Transwell® -96 Well Plate 0.4 μm Polycarbonate Membrane, Corning, Sigma-Aldrich) or physically separated from the T-B coculture in the top compartment in the presence of 25 μg/ml anti-IL-6Rα (MR16-1) or 25 μg/ml rat IgG2a (clone 2A3; Bio X Cell). Additionally, 125,000 $Ly6G^+CD11b^+$ cells alone were either stimulated with 50 ng/ml IL-6 (Miltenyi Biotec) or equimolar amounts of human IL-6-IL-6Rα (a kind gift of Stefan Rose-John, Kiel, Germany) in the presence of 25 μg/ml anti-IL-6Rα or 25 μg/ml rat IgG2a. After 20 h, cells were analyzed for pSTAT3 using the BD Phosflow™ Lyse/Fix Buffer and BD Phosflow™ Perm Buffer III (BD Biosciences) according to the manufacturer's instructions and stained with fluorochrome-conjugated anti-mouse STAT3 pY705 (4/P-STAT3), CD4 (RM4-5), CD11b (M1/70), CD19 (1D3), and Ly6G (1A8). Flow cytometric analysis was performed on a CytoFLEX flow cytometer (Beckman Coulter, Brea, USA) and flow cytometric data were analyzed using FlowJo software (Tree Star, Ashland, USA). FACS sorting was performed on a FACS Aria III (BD Biosciences).

Arg1 enzyme activity assay

A total of 50,000 $Ly6G^+$ cells were FACS-purified from the CNS of *Ly6g*$^{Cre/WT}$ mice. All samples underwent post-sort purity control, samples with purity < 90% were dismissed. Total protein was extracted using the CelLytic MT Cell Lysis Reagent (C3228, Sigma-Aldrich) from sorted cells according to the manufacturer's instructions. Arg1 enzyme activity was analyzed using the Arginase Activity Assay Kit (MAK112, Sigma-Aldrich) according to the manufacturer's instructions, all biological samples were divided into three technical replicates.

Histology and cytology

Mice were perfused with cold PBS followed by 4% paraformaldehyde fixation (pH 7.4). Cerebrum, brainstem, spinal cord, and optic nerve tissues were dissected and embedded in paraffin. Antigen retrieval was performed on 3 μm thick sections according to standardized protocols by heating with citrate buffer (pH6). Endogenous peroxidases (peroxidase blocking reagent, Dako) were neutralized and unspecific binding blocked for 5 min (PBS/1% BSA/2% FCS). For brightfield microscopy, tissue sections were incubated with rat-anti-mouse B220 (clone RA3-6B2). Bound primary antibodies were visualized with biotin-labeled anti-rat antibody and streptavidin-peroxidase staining method using polymerized 3,3'-diaminobenzidine (all reagents from Dako; haemalaun counterstaining of nuclei). For immunofluorescence, sections were blocked for 5 min (PBS/1% BSA/2% FCS) and subsequently incubated with mouse rat-anti Ly6G (clone 1A8). Bound primary antibodies were visualized by using goat-anti-rabbit-HRP and tyramide signal amplification (TSA) (Alexa488, life Technologies). Subsequently, sections were incubated with rabbit anti-pSTAT3 (clone D3A7, Cell Signalling Technology) and bound antibodies were visualized with Alexa555-labeled-goat anti-rabbit antibody. Finally, slides were incubated with 647-labeled rat-anti-B220 (clone RA3-6B2) and nuclei were stained with 4',6-diamidino-2-phenylindole (DAPI, Invitrogen). For further stainings, rat anti-mouse CD19 (clone 60MP31, eBioscience) and polyclonal rabbit anti-mouse CD3 (Dako) were used. Immunostained sections were scanned using Pannoramic Digital Slide Scanner 250 FLASH II (3DHistech) in 200x magnification. For cytology, cells were highly purified *ex vivo* by FACS sorting. After Cytospin™ centrifugation (Thermo Fisher), May-Gruenwald-Giemsa staining was performed according to the manufacturer's instructions (Merck).

Quantitative PCR

Total RNA was isolated with RNAeasy Plus micro kit (Qiagen, Hilden, Germany). The isolated RNA was transcribed into cDNA using the TaqMan Reverse Transcription Reagents Kit (Life Technologies, Carlsbad, USA) according to the manufacturer's instructions. Probes were purchased from Life Technologies and the assays were performed on 96-well reaction plates (Life Technologies). The real time PCR was performed on StepOnePlus system (Life Technologies). In all experiments *Actb* was used as reference gene to normalize gene expression, all samples were run as triplicates.

RNA-seq

Total RNA was isolated with RNAeasy Plus micro kit (Qiagen). Quality and integrity of total RNA was controlled on Agilent Technologies 2100 Bioanalyzer (Agilent Technologies, Santa Clara, USA). RNAseq analysis: library preparation for bulk 3'-sequencing of poly(A)-RNA was done as described previously 57. Briefly, barcoded cDNA of each sample was generated with a Maxima RT polymerase (Thermo Fisher) using oligo-dT primer containing barcodes, unique molecular identifiers (UMIs) and an adapter. 5' ends of the cDNAs were extended by a template switch oligo (TSO) and full-length cDNA was amplified with primers binding to the TSO-site and the adapter. cDNA was tagmented with the Nextera XT kit (Illumina, San Diego, USA) and 3'-end-fragments finally amplified using primers with Illumina P5 and P7 overhangs. In comparison to Parekh *et al.* 57, the P5 and P7 sites were exchanged to allow sequencing of the cDNA in read1 and barcodes and UMIs in read2 to achieve a better cluster recognition. The library was sequenced on a NextSeq 500 (Illumina) with 75 cycles for the cDNA in read1 and 16 cycles for the barcodes and UMIs in read2. Data were processed using the published Drop-seq pipeline (v1.0) to generate sample- and gene-wise UMI tables 58. Reference genome (GRCm38) was used for alignment. Transcript and gene definitions were used according to the ENSEMBL annotation release 91. Differential gene expression analysis was conducted with DESeq v1.18.1. 59. After fitting a model with all samples, constrasts of interest were extracted. Expression differences between CNS onset and the remaining samples were determined. Then contrasts between all possible pairwise combinations of the other groups, except the CNS onset-samples, were extracted. Genes exclusively regulated in the CNS onset-group were subjected to pathway analysis with GOrilla 60. We considered genes with an FDR <= 0.05 and an at least twofold absolute expression difference between groups to be differentially expressed. For PCA analysis the top 2000 variable genes were used as input.

Statistics

Statistical evaluations of cell frequency measurements, cell numbers, mRNA amounts, chemokine levels or enzyme activity were performed with the unpaired Student's t test or Mann Whitney U test as indicated in the figure legends when two populations were compared. Two-tailed p-values < 0.05 were considered significant. Multiple comparisons were performed with one-way ANOVA and post-hoc multiple comparisons tests as indicated in the legends to the figures. EAE scores between groups were analyzed as disease burden per individual day with two-way ANOVA and Bonferroni's post-testing. A p-value of $p<0.05$ was considered significant. If not otherwise stated, values are given as mean ± standard deviation (s.d.). Calculations were performed using Graph Pad Prism v7.04 (Graph-Pad software, La Jolla, USA) or R software (R Core Team 2015, version 3.5.1).

Supplementary Material

Refer to Web version on PubMed Central for supplementary material.

Acknowledgments

We would like to thank all members of the Korn Group and especially V. Husterer for her skillful technical assistance. This work was supported by the Deutsche Forschungsgemeinschaft (SFB1054-B06 to TK, TRR128 to

TK, SyNergy to TK, Kompetenznetz Multiple Sklerose KKNMS to BK), the German Ministry of Education and Research (BMBF, T-B in NMO to TK), and by the ERC (CoG 647215 to TK). BK received intramural funding from the Technical University of Munich. LA is supported by a clinical scientist program provided by the Deutsche Forschungsgemeinschaft (Synergy). DM is supported by the Swiss National Science foundation.

References

1. Lappat EJ, Cawein M. A Study of the Leukemoid Response to Transplantable A-280 Tumor in Mice. Cancer Res. 1964; 24:302–311. [PubMed: 14115699]
2. Bronte V, et al. Recommendations for myeloid-derived suppressor cell nomenclature and characterization standards. Nature communications. 2016; 7 12150.
3. Condamine T, et al. Lectin-type oxidized LDL receptor-1 distinguishes population of human polymorphonuclear myeloid-derived suppressor cells in cancer patients. Science immunology. 2016; 1
4. Dufait I, et al. Signal transducer and activator of transcription 3 in myeloid-derived suppressor cells: an opportunity for cancer therapy. Oncotarget. 2016; 7:42698–42715. [PubMed: 27029037]
5. Lelis FJN, et al. Myeloid-derived suppressor cells modulate B-cell responses. Immunol Lett. 2017; 188:108–115. [PubMed: 28687234]
6. Li Y, et al. Myeloid-derived suppressor cells as a potential therapy for experimental autoimmune myasthenia gravis. J Immunol. 2014; 193:2127–2134. [PubMed: 25057008]
7. Park M-J, et al. Myeloid-Derived Suppressor Cells Induce the Expansion of Regulatory B Cells and Ameliorate Autoimmunity in the Sanroque Mouse Model of Systemic Lupus Erythematosus. Arthritis Rheumatol. 2016; 68:2717–2727. [PubMed: 27214349]
8. Xu X, et al. Myeloid-derived suppressor cells promote B-cell production of IgA in a TNFR2-dependent manner. Cell Mol Immunol. 2017; 14:597–606. [PubMed: 27133471]
9. Wang C, et al. Myeloid-Derived Suppressor Cells Inhibit T Follicular Helper Cell Immune Response in Japanese Encephalitis Virus Infection. J Immunol. 2017; 199:3094–3105. [PubMed: 28978693]
10. Flach A-C, et al. Autoantibody-boosted T-cell reactivation in the target organ triggers manifestation of autoimmune CNS disease. Proc Natl Acad Sci USA. 2016; 113:3323–3328. [PubMed: 26957602]
11. Molnarfi N, et al. MHC class II-dependent B cell APC function is required for induction of CNS autoimmunity independent of myelin-specific antibodies. J Exp Med. 2013; 210:2921–2937. [PubMed: 24323356]
12. Hauser SL, et al. B-cell depletion with rituximab in relapsing-remitting multiple sclerosis. N Engl J Med. 2008; 358:676–688. [PubMed: 18272891]
13. Li R, et al. Proinflammatory GM-CSF-producing B cells in multiple sclerosis and B cell depletion therapy. Sci Transl Med. 2015; 7:310ra166.
14. Magliozzi R, et al. Meningeal B-cell follicles in secondary progressive multiple sclerosis associate with early onset of disease and severe cortical pathology. Brain. 2007; 130:1089–1104. [PubMed: 17438020]
15. Gotot J, et al. Regulatory T cells use programmed death 1 ligands to directly suppress autoreactive B cells in vivo. Proc Natl Acad Sci USA. 2012; 109:10468–10473. [PubMed: 22689978]
16. Nakamura K, Kitani A, Strober W. Cell contact-dependent immunosuppression by CD4(+)CD25(+) regulatory T cells is mediated by cell surface-bound transforming growth factor beta. J Exp Med. 2001; 194:629–644. [PubMed: 11535631]
17. Jang E, et al. Foxp3+ regulatory T cells control humoral autoimmunity by suppressing the development of long-lived plasma cells. J Immunol. 2011; 186:1546–1553. [PubMed: 21209284]
18. Koutrolos M, Berer K, Kawakami N, Wekerle H, Krishnamoorthy G. Treg cells mediate recovery from EAE by controlling effector T cell proliferation and motility in the CNS. Acta neuropathologica communications. 2014; 2:163. [PubMed: 25476447]
19. Bennett JL, et al. B lymphocytes in neuromyelitis optica. Neurol Neuroimmunol Neuroinflamm. 2015; 2:e104–e104. [PubMed: 25977932]
20. Cepok S, et al. Short-lived plasma blasts are the main B cell effector subset during the course of multiple sclerosis. Brain. 2005; 128:1667–1676. [PubMed: 15800022]

21. Gold R, Linington C, Lassmann H. Understanding pathogenesis and therapy of multiple sclerosis via animal models: 70 years of merits and culprits in experimental autoimmune encephalomyelitis research. Brain. 2006; 129:1953–1971. [PubMed: 16632554]
22. Hasenberg A, et al. Catchup: a mouse model for imaging-based tracking and modulation of neutrophil granulocytes. Nat Methods. 2015; 12:445–452. [PubMed: 25775045]
23. Marigo I, et al. Tumor-induced tolerance and immune suppression depend on the C/EBPbeta transcription factor. Immunity. 2010; 32:790–802. [PubMed: 20605485]
24. Durant L, et al. Diverse targets of the transcription factor STAT3 contribute to T cell pathogenicity and homeostasis. Immunity. 2010; 32:605–615. [PubMed: 20493732]
25. Gabrilovich DI, Nagaraj S. Myeloid-derived suppressor cells as regulators of the immune system. Nat Rev Immunol. 2009; 9:162–174. [PubMed: 19197294]
26. Veglia F, Perego M, Gabrilovich D. Myeloid-derived suppressor cells coming of age. Nat Immunol. 2018; 19:108–119. [PubMed: 29348500]
27. Yanaba K, et al. A regulatory B cell subset with a unique CD1dhiCD5+ phenotype controls T cell-dependent inflammatory responses. Immunity. 2008; 28:639–650. [PubMed: 18482568]
28. Rauch PJ, et al. Innate response activator B cells protect against microbial sepsis. Science (New York, NY). 2012; 335:597–601.
29. Litzenburger T, et al. B lymphocytes producing demyelinating autoantibodies: development and function in gene-targeted transgenic mice. J Exp Med. 1998; 188:169–180. [PubMed: 9653093]
30. Bettelli E, et al. Myelin oligodendrocyte glycoprotein-specific T cell receptor transgenic mice develop spontaneous autoimmune optic neuritis. J Exp Med. 2003; 197:1073–1081. [PubMed: 12732654]
31. Weber MS, et al. B-cell activation influences T-cell polarization and outcome of anti-CD20 B-cell depletion in central nervous system autoimmunity. Annals of neurology. 2010; 68:369–383. [PubMed: 20641064]
32. Krasemann S, et al. The TREM2-APOE Pathway Drives the Transcriptional Phenotype of Dysfunctional Microglia in Neurodegenerative Diseases. Immunity. 2017; 47:566–581.e9. [PubMed: 28930663]
33. Tak T, Tesselaar K, Pillay J, Borghans JAM, Koenderman L. What's your age again? Determination of human neutrophil half-lives revisited. J Leukoc Biol. 2013; 94:595–601. [PubMed: 23625199]
34. Pierson ER, Wagner CA, Goverman JM. The contribution of neutrophils to CNS autoimmunity. Clin Immunol. 2018; 189:23–28. [PubMed: 27377536]
35. Lévesque SA, et al. Myeloid cell transmigration across the CNS vasculature triggers IL-1β-driven neuroinflammation during autoimmune encephalomyelitis in mice. J Exp Med. 2016; 213:929–949. [PubMed: 27139491]
36. Steinbach K, Piedavent M, Bauer S, Neumann JT, Friese MA. Neutrophils amplify autoimmune central nervous system infiltrates by maturing local APCs. J Immunol. 2013; 191:4531–4539. [PubMed: 24062488]
37. Soulika AM, et al. Initiation and progression of axonopathy in experimental autoimmune encephalomyelitis. J Neurosci. 2009; 29:14965–14979. [PubMed: 19940192]
38. Cheretakis C, Leung R, Sun CX, Dror Y, Glogauer M. Timing of neutrophil tissue repopulation predicts restoration of innate immune protection in a murine bone marrow transplantation model. Blood. 2006; 108:2821–2826. [PubMed: 16804110]
39. Carlson T, Kroenke M, Rao P, Lane TE, Segal B. The Th17-ELR+ CXC chemokine pathway is essential for the development of central nervous system autoimmune disease. J Exp Med. 2008; 205:811–823. [PubMed: 18347102]
40. Bartosik-Psujek H, Stelmasiak Z. The levels of chemokines CXCL8, CCL2 and CCL5 in multiple sclerosis patients are linked to the activity of the disease. Eur J Neurol. 2005; 12:49–54. [PubMed: 15613147]
41. Rumble JM, et al. Neutrophil-related factors as biomarkers in EAE and MS. J Exp Med. 2015; 212:23–35. [PubMed: 25559893]
42. Däbritz J, Judd LM, Chalinor HV, Menheniott TR, Giraud AS. Altered gp130 signalling ameliorates experimental colitis via myeloid cell-specific STAT3 activation and myeloid-derived suppressor cells. Sci Rep. 2016; 6 20584.

43. Arocena AR, et al. Myeloid-derived suppressor cells are key players in the resolution of inflammation during a model of acute infection. Eur J Immunol. 2014; 44:184–194. [PubMed: 24166778]
44. Heink S, et al. Trans-presentation of IL-6 by dendritic cells is required for the priming of pathogenic TH17 cells. Nat Immunol. 2017; 18:74–85. [PubMed: 27893700]
45. Zehntner SP, et al. Neutrophils that infiltrate the central nervous system regulate T cell responses. J Immunol. 2005; 174:5124–5131. [PubMed: 15814744]
46. Hjelmström P, Juedes AE, Fjell J, Ruddle NH. B-cell-deficient mice develop experimental allergic encephalomyelitis with demyelination after myelin oligodendrocyte glycoprotein sensitization. J Immunol. 1998; 161:4480–4483. [PubMed: 9794370]
47. Magliozzi R, Columba-Cabezas S, Serafini B, Aloisi F. Intracerebral expression of CXCL13 and BAFF is accompanied by formation of lymphoid follicle-like structures in the meninges of mice with relapsing experimental autoimmune encephalomyelitis. J Neuroimmunol. 2004; 148:11–23. [PubMed: 14975582]
48. Matsushita T, Horikawa M, Iwata Y, Tedder TF. Regulatory B cells (B10 cells) and regulatory T cells have independent roles in controlling experimental autoimmune encephalomyelitis initiation and late-phase immunopathogenesis. J Immunol. 2010; 185:2240–2252. [PubMed: 20624940]
49. Shen P, et al. IL-35-producing B cells are critical regulators of immunity during autoimmune and infectious diseases. Nature. 2014; 507:366–370. [PubMed: 24572363]
50. Pöllinger B, et al. Spontaneous relapsing-remitting EAE in the SJL/J mouse: MOG-reactive transgenic T cells recruit endogenous MOG-specific B cells. J Exp Med. 2009; 206:1303–1316. [PubMed: 19487416]
51. Polman CH, et al. Diagnostic criteria for multiple sclerosis: 2010 revisions to the McDonald criteria. Annals of neurology. 2011; 69:292–302. [PubMed: 21387374]
52. Shen FW, et al. Cloning of Ly-5 cDNA. Proceedings of the National Academy of Sciences. 1985; 82:7360–7363.
53. Betz UA, et al. Postnatally induced inactivation of gp130 in mice results in neurological, cardiac, hematopoietic, immunological, hepatic, and pulmonary defects. J Exp Med. 1998; 188:1955–1965. [PubMed: 9815272]
54. Takeda K, et al. Stat3 activation is responsible for IL-6-dependent T cell proliferation through preventing apoptosis: generation and characterization of T cell-specific Stat3-deficient mice. J Immunol. 1998; 161:4652–4660. [PubMed: 9794394]
55. Wunderlich FT, et al. Interleukin-6 signaling in liver-parenchymal cells suppresses hepatic inflammation and improves systemic insulin action. Cell Metab. 2010; 12:237–249. [PubMed: 20816090]
56. Anderson KG, et al. Intravascular staining for discrimination of vascular and tissue leukocytes. Nat Protoc. 2014; 9:209–222. [PubMed: 24385150]
57. Parekh S, Ziegenhain C, Vieth B, Enard W, Hellmann I. The impact of amplification on differential expression analyses by RNA-seq. Sci Rep. 2016; 6 25533.
58. Macosko EZ, et al. Highly Parallel Genome-wide Expression Profiling of Individual Cells Using Nanoliter Droplets. Cell. 2015; 161:1202–1214. [PubMed: 26000488]
59. Love MI, Huber W, Anders S. Moderated estimation of fold change and dispersion for RNA-seq data with DESeq2. Genome Biol. 2014; 15:550. [PubMed: 25516281]
60. Eden E, Navon R, Steinfeld I, Lipson D, Yakhini Z. GOrilla: a tool for discovery and visualization of enriched GO terms in ranked gene lists. BMC Bioinformatics. 2009; 10:48. [PubMed: 19192299]

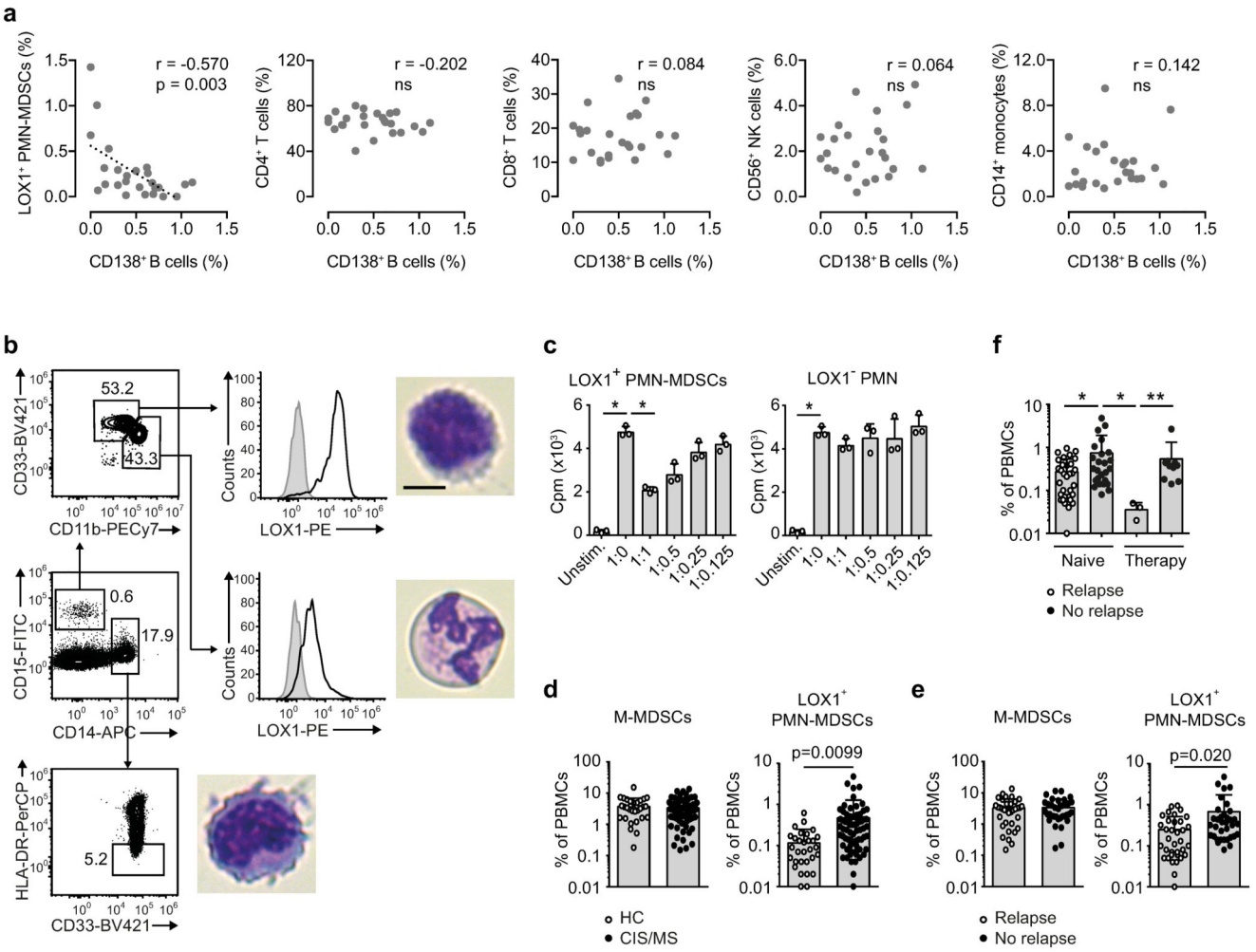

Figure 1. LOX1^{+} PMN-MDSCs in the CSF are negatively correlated with intrathecal CD138^{+} B cells in patients with MS and indicate stable disease.

a, Correlation of CD19^{+}CD138^{+}HLA-DR^{+} B cells with LOX1^{+} PMN-MDSCs, CD4^{+} T helper cells, CD8^{+} cytotoxic T cells, CD3^{-}CD19^{-}CD56^{+} natural killer (NK) cells, and CD3^{-}CD19^{-}CD14^{+} monocytes in the CSF of therapy naïve patients with relapsing remitting MS or clinically isolated syndrome (CIS) (n=25); symbols depict individual patients; not significant (ns); Spearman's r analysis. **b,** Flow-cytometry analysis and May-Gruenwald-Giemsa staining of granulocytic CD15^{+}CD11b^{int}CD33^{high}LOX1^{high}, CD15^{+}CD11b^{high}CD33^{low}LOX1^{low} and monocytic CD15^{-}CD14^{+}HLA-DR^{low} (M-MDSCs) cells from the blood mononuclear cell (PBMC) compartment of MS patients; grey histograms depict isotype controls; representative of five independent experiments; scale bar 5 μm; gate on live single cells. **c,** ^{3}H-thymidine incorporation of CD40 antibody- and IL-4-stimulated CD19^{+}CD27^{-} B cells upon co-culture in descending ratios with CD15^{+}CD11b^{int}CD33^{high}LOX1^{high} PMN-MDSCs from PBMCs and CD15^{+}CD11b^{high}CD33^{low} LOX1^{low} neutrophils from whole blood samples; symbols depict counts per minute (cpm, mean + s.d.) of three replicate wells; representative plots of two independent experiments; Kruskal-Wallis test with Dunn's post test; *p<0.05. **d,** Frequencies

of M-MDSCs and LOX1^{+} PMN-MDSCs in PBMCs of healthy control individuals (HC, n=31) and MS/CIS patients (n=70); symbols depict individual patients (bars mean + s.d.); Mann-Whitney U test, corrected for age. **e,** Frequencies of M-MDSCs and LOX1^{+} PMN-MDSCs in PBMCs of CIS/MS patients during acute relapse (relapse, n=35, 51.4% female, age 31 ± 9 years, disease duration 22 ± 44 months) or in stable patients (no relapse, n=35, 65.7% female, age 42 ± 12 years, disease duration 68 ± 97 months); symbols depict individual patients (bars mean + s.d.), Mann-Whitney U test, corrected for age. **f,** Frequencies of LOX1^{+} PMN-MDSCs in PBMCs of therapy naïve patients during acute relapse (naïve relapse, n=32) or with stable disease (naïve no relapse, n=25) and of patients under immunosuppressive therapy that suffered from acute relapse (therapy, relapse n=3) or were stable (therapy, no relapse n=10); symbols depict individual patients (bars mean ± SD); Kruskal-Wallis test with Dunn's post test, corrected for age; *p<0.05, **p<0.01.

Europe PMC Funders Author Manuscripts

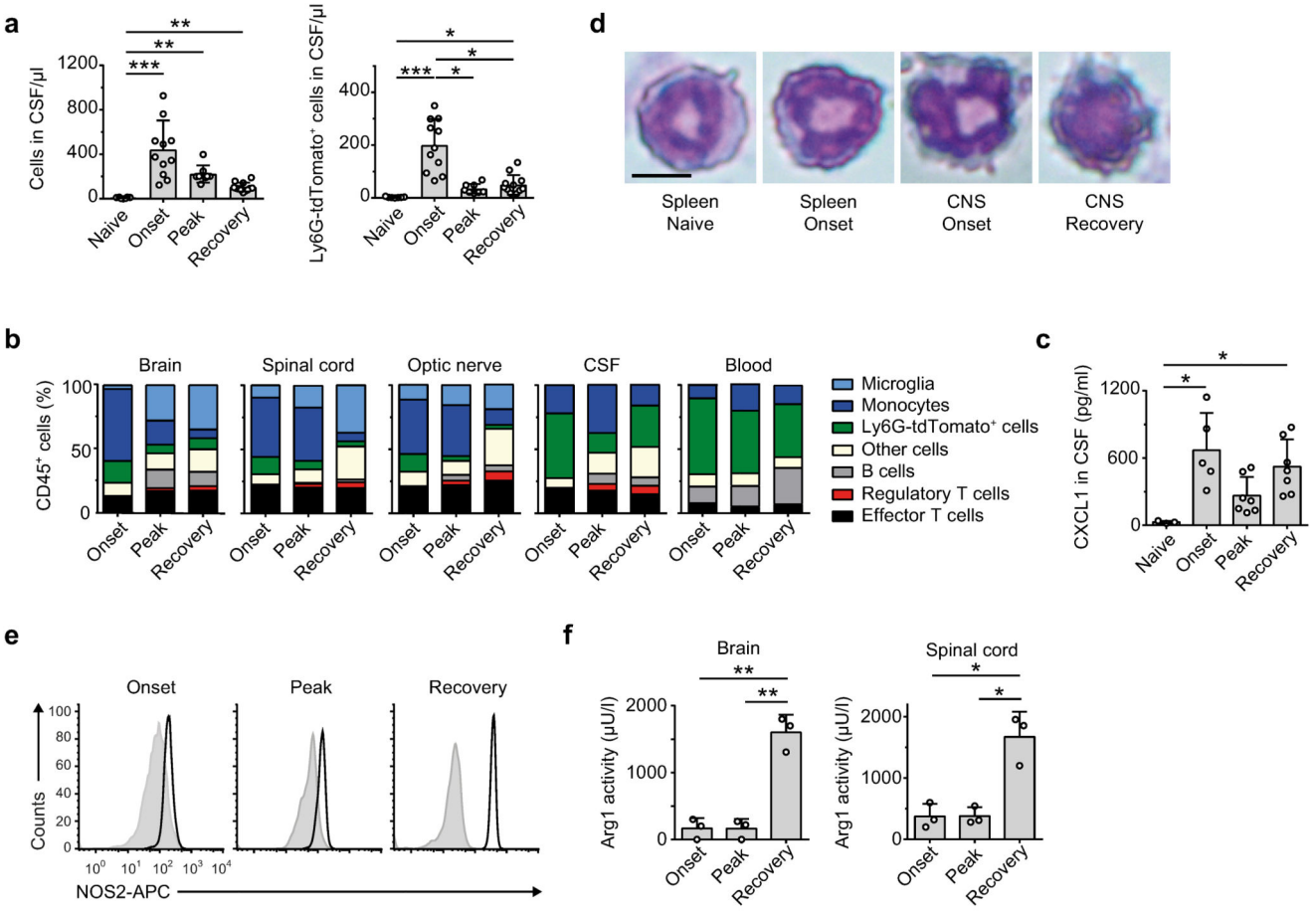

Figure 2. Population dynamics and phenotype of Ly6G$^+$ neutrophils within different compartments in the course of EAE.

a, CSF total cell and Ly6G-tdTomato$^+$ cell counts during different EAE phases in *Ly6g*$^{Cre/WT}$ mice; naïve n=6, onset n=11, peak n=8, recovery n=12; symbols depict individual mice (bars mean + s.d.); data were pooled from four independent experiments; Kruskal-Wallis test with Dunn's post test; *p<0.05, **p<0.01, ***p<0.001. **b,** Population dynamics of CD4$^+$Foxp3$^-$ effector T cells, CD4$^+$Foxp3$^+$ regulatory T cells, CD19$^+$ B cells, Ly6G-tdTomato$^+$ cells, CD45^{high}CD11b$^+$ monocytes and CD45^{int}CD11b$^+$ microglia purified from brain, spinal cord, optic nerve, CSF, and blood during EAE onset, peak, and recovery in *Ly6g*$^{Cre/WT}$ mice (n=4 per time point); bars depict mean values of different cell subsets from pooled *Ly6g*$^{Cre/WT}$ mice. **c,** Analysis of CXCL1 levels in the CSF of *Ly6g*$^{Cre/WT}$ mice during different EAE phases; naïve=3, onset n=5, peak n=7, recovery n=7; symbols depict individual mice (bars mean + s.d.), Kruskal-Wallis test with Dunn's post test; *p<0.05. **d,** May-Gruenwald-Giemsa staining of Ly6G-tdTomato$^+$ cells from naïve spleen, spleen during EAE onset, CNS during EAE onset, and CNS during EAE recovery; representative of six individual mice; scale bar 5 µm. **e,** Flow-cytometry analysis of intracellular NOS2 in Ly6G-tdTomato$^+$ cells from spinal cords of EAE mice at onset, peak, and recovery; representative of 6 mice per time point; gate on CD11b$^+$Ly6G$^+$ cells. **f,** Arginase 1 (Arg1) enzyme activity assay with Ly6G-tdTomato$^+$ cells *ex vivo* from brain and spinal cord of *Ly6g*$^{Cre/WT}$ mice at

Europe PMC Funders Author Manuscripts

EAE onset, peak, and recovery; symbols depict individual mice (bars mean + s.d.); Kruskal-Wallis test with Dunn's post test; *p<0.05, **p<0.01.

Europe PMC Funders Author Manuscripts

Europe PMC Funders Author Manuscripts

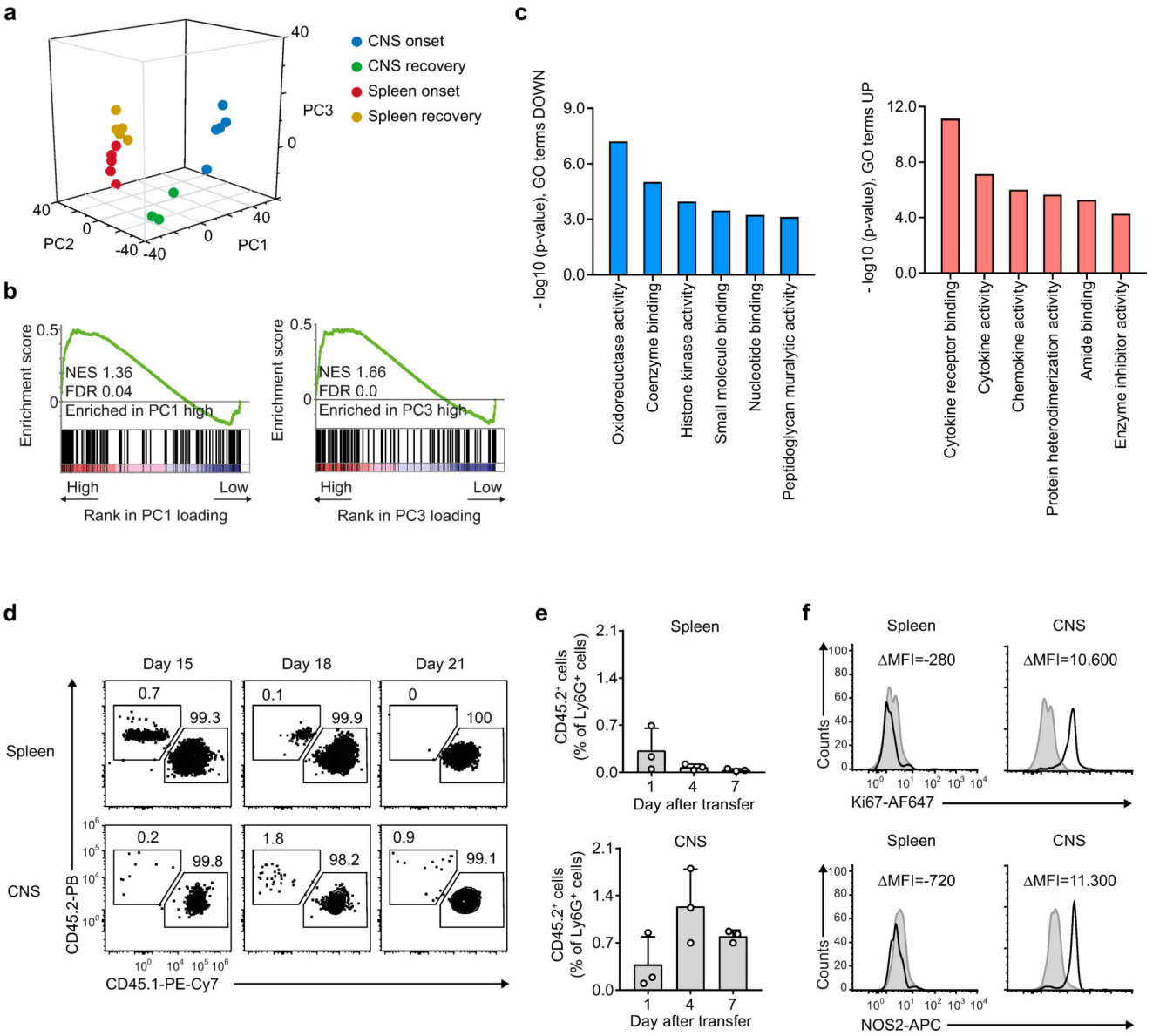

Figure 3. In the EAE model, the generation of PMN-MDSCs is restricted to the inflamed CNS.

a-c, RNA-seq analysis of Ly6G-tdTomato^{+} cells from the spleen and the CNS of *Ly6g*$^{Cre/WT}$ mice at different stages of EAE (onset d13, early recovery d22). **a,** 3D principal component analysis of gene expression in Ly6G-tdTomato^{+} cells; symbols represent individual mice, colored by condition. **b,** Gene set enrichment analysis (GSEA) of a human PMN-MDSC-signature 3 in murine Ly6G-tdTomato^{+} populations according to their rank in PC1 and PC3. **c,** Analysis of universally downregulated or upregulated genes in CNS onset-Ly6G^{+} cells vs all other Ly6G^{+} populations. Plot of the top 6 overrepresented gene ontology terms (focus on 'function' in GOrilla), sorted by -log10 (p-value). **d-f,** Adoptive transfer of Ly6G-tdTomato^{+} cells from the spleen of immunized *Ly6g*$^{Cre/WT}$ donor mice (CD45.2^{+}) (d7) and transferred into congenic (CD45.1^{+}) hosts that had been immunized for EAE 14 days earlier. **d, e,** Flow-cytometry analysis (d) and frequencies (e) of transferred Ly6G^{+} cells donor cells (CD45.2^{+})

re-isolated from spleens and CNS of recipient mice ($CD45.1^+$) on days 1 (d15 after immunization), 4 (d18), and 7 (d 21) after transfer; symbols depict individual mice (bars mean + s.d., n=3 per time point); gate on live single $Ly6G^+$ cells. **f,** Intracellular staining for Ki67 (proliferation) and NOS2 in transferred $Ly6G^+$ cells re-isolated from spleen and CNS on day 4 after transfer; spleen and CNS plots were generated from 3 pooled mice; numbers in the histograms indicate difference in mean fluorescence intensity as compared to FMO (ΔMFI); gate on $Ly6G^+CD45.2^+CD45.1^-$ (donor) cells.

Europe PMC Funders Author Manuscripts

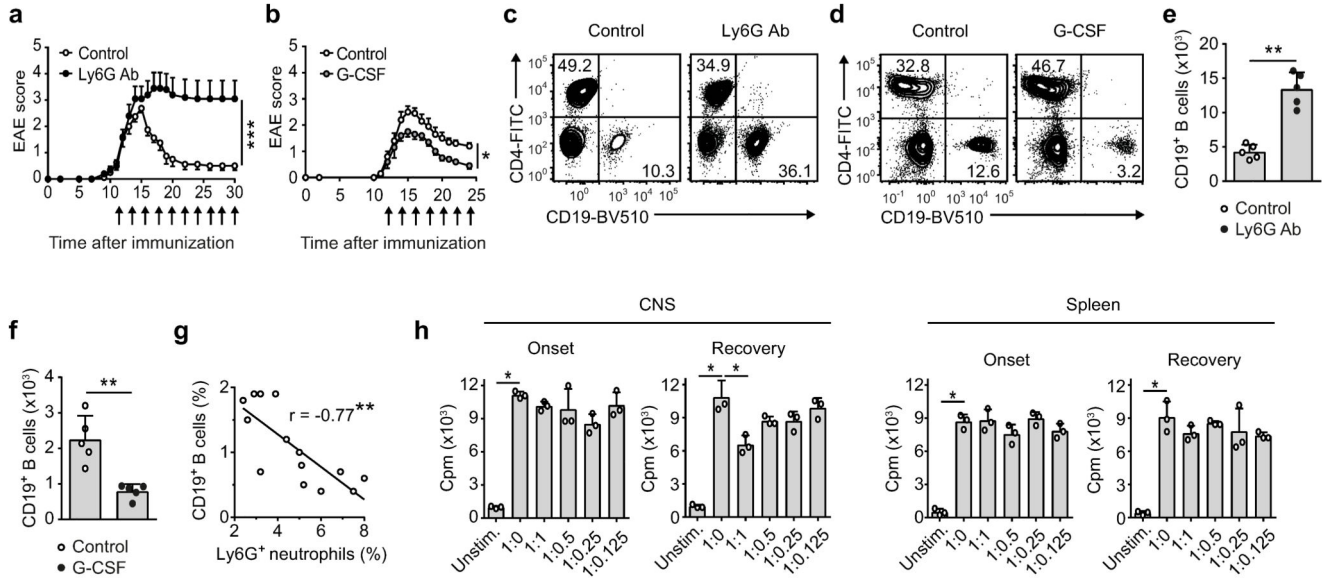

Figure 4. PMN-MDSCs contribute to inducing recovery from EAE.

a, EAE disease course in *Ly6g*$^{Cre/WT}$ mice treated with 400 μg of Ly6G antibody (Ly6G Ab, n=10) or rat IgG2a control antibody (Control, n=8) i.p. every other day (highlighted by arrows), starting on d12 after EAE induction; symbols depict means and s.d.; two-way ANOVA with Bonferroni's multiple comparison; ***p<0.001; representative disease course of three independent experiments. **b,** EAE disease course in *Ly6g*$^{Cre/WT}$ mice treated with 200 μg/kg G-CSF (G-CSF, n=5) or control 5% glucose (Control, n=5) i.p. every other day (highlighted by arrows), starting on d12 after immunization; symbols depict means and s.d.; two-way ANOVA with Bonferroni's multiple comparison; *p<0.05. **c,** Flow-cytometry analysis of CD19$^+$ B cells and CD4$^+$ T cells within the CD11b$^-$ lymphoid compartment purified at early disease recovery (d22) from spinal cords of *Ly6g*$^{Cre/WT}$ mice treated with control IgG or Ly6G antibody; representative plots of 5 mice from each group; gate on live CD45.2$^+$CD11b$^-$ cells. **d,** Flow-cytometry analysis of CD19$^+$ B cells and CD4$^+$ T cells within the CD11b$^-$ lymphoid compartment purified at early disease recovery (d21) from spinal cords of *Ly6g*$^{Cre/WT}$ mice control-treated or treated with G-CSF; representative plots of 5 mice from each group; gate on live CD45.2$^+$CD11b$^-$ cells. **e,** Total number of CD19$^+$ B cells purified at early disease recovery (d22) from spinal cords of *Ly6g*$^{Cre/WT}$ mice treated with control antibody (Control, n=5) or Ly6G antibody (Ly6G Ab, n=5); symbols depict individual mice (bars mean + s.d.); Mann-Whitney U test; **p<0.01. **f,** Total number of CD19$^+$ B cells purified at early disease recovery (d21) from spinal cords of *Ly6g*$^{Cre/WT}$ mice control-treated or treated with G-CSF; symbols depict individual mice (bars mean ± SD); Mann-Whitney U test; **p<0.01. **g,** Correlation of CD19$^+$ B cell and Ly6G$^+$ MDSC frequencies in the spinal cord of G-CSF-treated and control-treated *Ly6g*$^{Cre/WT}$ mice at early disease recovery (d21); symbols depict individual mice; Spearman's r; **p<0.01. **h,** ^{3}H-thymidine incorporation of CD40 antibody- and IL-4-stimulated CD19$^+$B220$^+$ B cells from spleens of naïve *Ly6g*$^{Cre/WT}$ mice upon co-culture in descending ratios with Ly6G$^+$ cells from the CNS and spleen of *Ly6g*$^{Cre/WT}$ EAE mice at disease onset (d12) and early recovery

(d20); symbols depict counts per minute (cpm, mean + s.d.) of three replicate wells; Kruskal-Wallis test with Dunn's post test; *p<0.05.

Europe PMC Funders Author Manuscripts

Europe PMC Funders Author Manuscripts

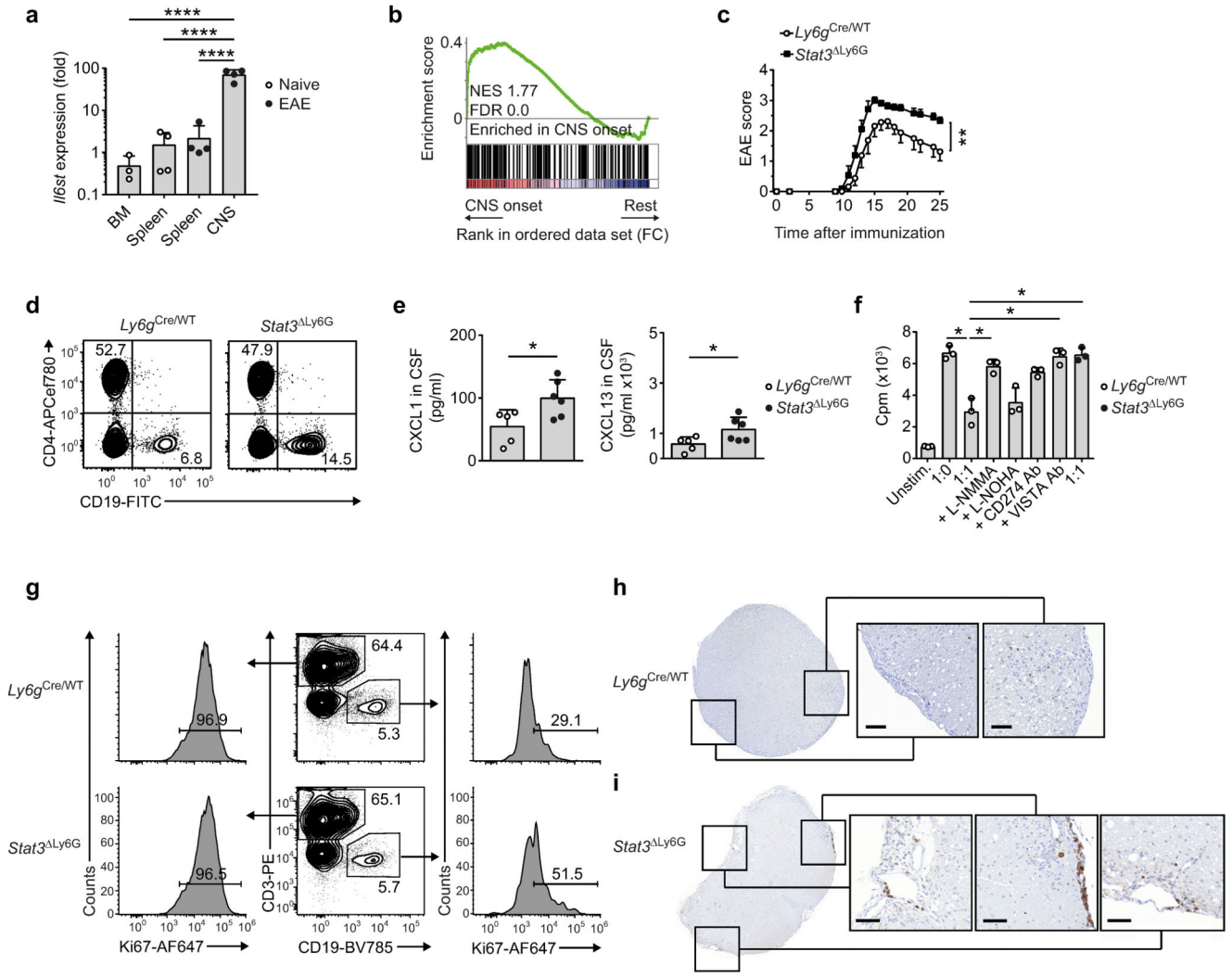

Figure 5. Ly6G$^+$ cells differentiate into MDSCs in the CNS in a STAT3-dependent manner.

a, qRT-PCR analysis of *Il6st* mRNA (which encodes gp130) in Ly6G$^+$ cells purified from naïve bone marrow (BM Naive, n=3), naïve spleen (Spleen Naive, n=4), and from spleen (Spleen EAE, n=4) and CNS (CNS EAE, n=4) of EAE mice (d17 after immunization); results are normalized relative to Ly6G$^+$ cells purified from naïve spleen; symbols depict individual mice (bars mean +s.d.); one-way-ANOVA with Tukey's post test; ****p<0.0001. **b,** Gene set enrichment analysis, testing a set of STAT3-targeted genes 24 on subsets of Ly6G$^+$ cells. **c,** EAE disease course in *Ly6g*$^{Cre/WT}$ (n=10) and *Stat3*$^{\Delta Ly6G}$ (n=14) mice; symbols depict means and s.d.; two-way ANOVA with Bonferroni's multiple comparison test; **p<0.01; representative disease course out of three independent experiments. **d,** Flow-cytometry analysis of CD19$^+$ B cells and CD4$^+$ T cells within the live CD45.2$^+$CD11b$^-$ lymphoid compartment in the spinal cord of *Ly6g*$^{Cre/WT}$ and *Stat3*$^{\Delta Ly6G}$ mice at early recovery (d24); representative plots of 8 mice in each group. **e,** Analysis of CXCL1 and CXCL13 protein levels in the CSF of *Ly6g*$^{Cre/WT}$ (n=5) and *Stat3*$^{\Delta Ly6G}$ (n=6) mice at early disease recovery (d24); symbols depict individual mice (bars mean + s.d.); Unpaired

Student's t-test; *p<0.05. **f,** ^{3}H-thymidine incorporation of CD40 antibody- and IL-4-stimulated CD19^{+}B220^{+} B cells from spleens of naïve *Ly6g*$^{Cre/WT}$ mice upon co-culture with-Ly6G^{+} cells from the CNS of *Ly6g*$^{Cre/WT}$ or *Stat3*$^{\Delta Ly6G}$ EAE mice at early recovery (d21) in the presence of L-NMMA, L-NOHA, CD274 antibody (CD274 Ab), VISTA antibody (VISTA Ab) or without any supplement; symbols depict counts per minute (cpm, mean + s.d.) of three replicate wells; Kruskal-Wallis test with Dunn's post test; *p<0.05. **g,** Flow-cytometry analysis of intracellular Ki67 in CD3^{+} T cells and CD19^{+} B cells among CNS CD11b^{-} cells of *Ly6g*$^{Cre/WT}$ or *Stat3*$^{\Delta Ly6G}$ mice at early disease recovery (d21); representative plots of 6 mice in each group. **h, i,** Accumulation of B cells in the meninges and CNS parenchyma of *Stat3*$^{\Delta Ly6G}$ mice. Immunohistochemical analysis of B220^{+} B cells from *Ly6g*$^{Cre/WT}$ control **(h)** and *Stat3*$^{\Delta Ly6G}$ EAE mice **(i)** at early recovery (d23); 20 x magnification, scale bar 100 μm; representative of 5 mice in each group.

Europe PMC Funders Author Manuscripts

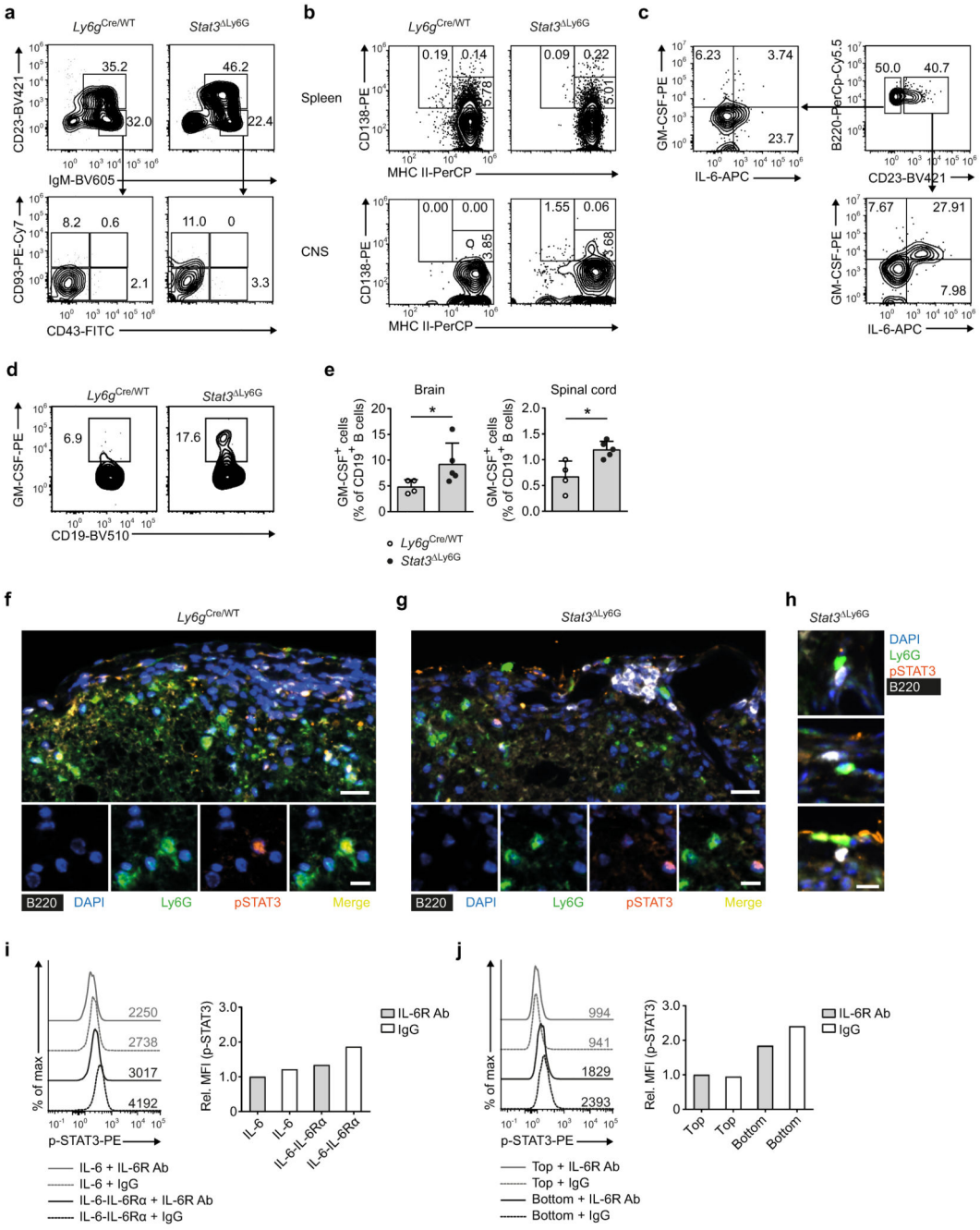

Figure 6. Ly6G$^+$ cells interact with B cells in the CNS.

a, Flow-cytometry analysis of CNS CD19$^+$B220$^+$ B cells from *Ly6g*$^{Cre/WT}$ control and *Stat3*$^{\Delta Ly6G}$ mice at early disease recovery (d21), showing the expression of IgM and CD23 (upper plots) and the expression of CD43 and CD93 on IgM$^+$CD23$^-$ gated B cells (lower plots); representative plots of 6 mice in each group. **b,** Flow-cytometry analysis of spleen (upper plots) and CNS (lower plots) CD19$^+$B220$^+$ B cells from *Ly6g*$^{Cre/WT}$ control and *Stat3*$^{\Delta Ly6G}$ mice at early disease recovery (d21), showing the expression of MHC-II and CD138; representative plots of 6 mice in each group. **c,** Flow-cytometry analysis of

Europe PMC Funders Author Manuscripts

intracellular IL-6 and GM-CSF in CNS $CD19^+B220^+$ B cells of $Ly6g^{Cre/WT}$ mice at at early disease recovery (d22) and stimulated *ex vivo* with PMA/ionomycin in the presence of brefeldin A, gated on $CD23^-$ (left upper plot) and $CD23^+$ (lower plot); representative plots of 7 mice. **d,** Flow-cytometry analysis of intracellular GM-CSF in *ex vivo* stimulated $CD19^+B220^+$ B cells from the brains of $Ly6g^{Cre/WT}$ control and $Stat3^{\Delta Ly6G}$ mice at early disease recovery (d23); representative plots of 4 ($Ly6g^{Cre/WT}$) and 5 ($Stat3^{\Delta Ly6G}$) mice in each group; gate on $CD45^+CD11b^-$ cells. **e,** Frequencies of GM-CSF producers within the $CD19^+B220^+$ B cell compartment from the brain and spinal cord of $Ly6g^{Cre/WT}$ (n=4) and $Stat3^{\Delta Ly6G}$ (n=5) mice at disease recovery (d23); symbols depict individual mice (bars mean + s.d.); Mann Whitney U test; *$p<0.05$. **f-h,** Immunofluorescence analysis using markers for neutrophils (Ly6G), B cells (B220) and phosphorylated STAT3 (pSTAT3) in spinal cord sections of $Ly6g^{Cre/WT}$ mice **(f)** and $Stat3^{\Delta Ly6G}$ mice **(g)** at early disease recovery (d23); scale bars 20 μm; higher power magnification of individual channels and merge in the lower rows of **(f)** and **(g)**; scale bars 10 μm. **h,** Examples of $Ly6G^+$ cells in close proximity of $B220^+$ B cells in the spinal cord of $Stat3^{\Delta Ly6G}$ mice during early recovery (d23); scale bar 10 μm. **i, j,** Flow-cytometry analysis of intracellular pSTAT3 in splenic $Ly6G^+$ cells. **i,** Exposure to IL-6 or IL-6-IL-6Rα in the presence of IL-6Rα antibody (IL-6R Ab) or control IgG; gate on $CD11b^+Ly6G^+$ cells; relative (rel.) MFI is normalized to the MFI of pSTAT3 in $Ly6G^+$ cells exposed to IL-6 in the presence of IL-6Rα antibody. **j,** $Ly6G^+$ cells were either added to the bottom compartment (together with a T and B cell co-culture) or to the top compartment (physically separated from the T and B cell co-culture) of a transwell system in the presence of IL-6Rα antibody or control IgG; gate on $CD11b^+Ly6G^+CD4^-CD19^-$ cells; relative MFI is normalized to the MFI of pSTAT3 in $Ly6G^+$ cells from the top compartment in the presence of anti-IL-6Rα; representative plots of two experiments.

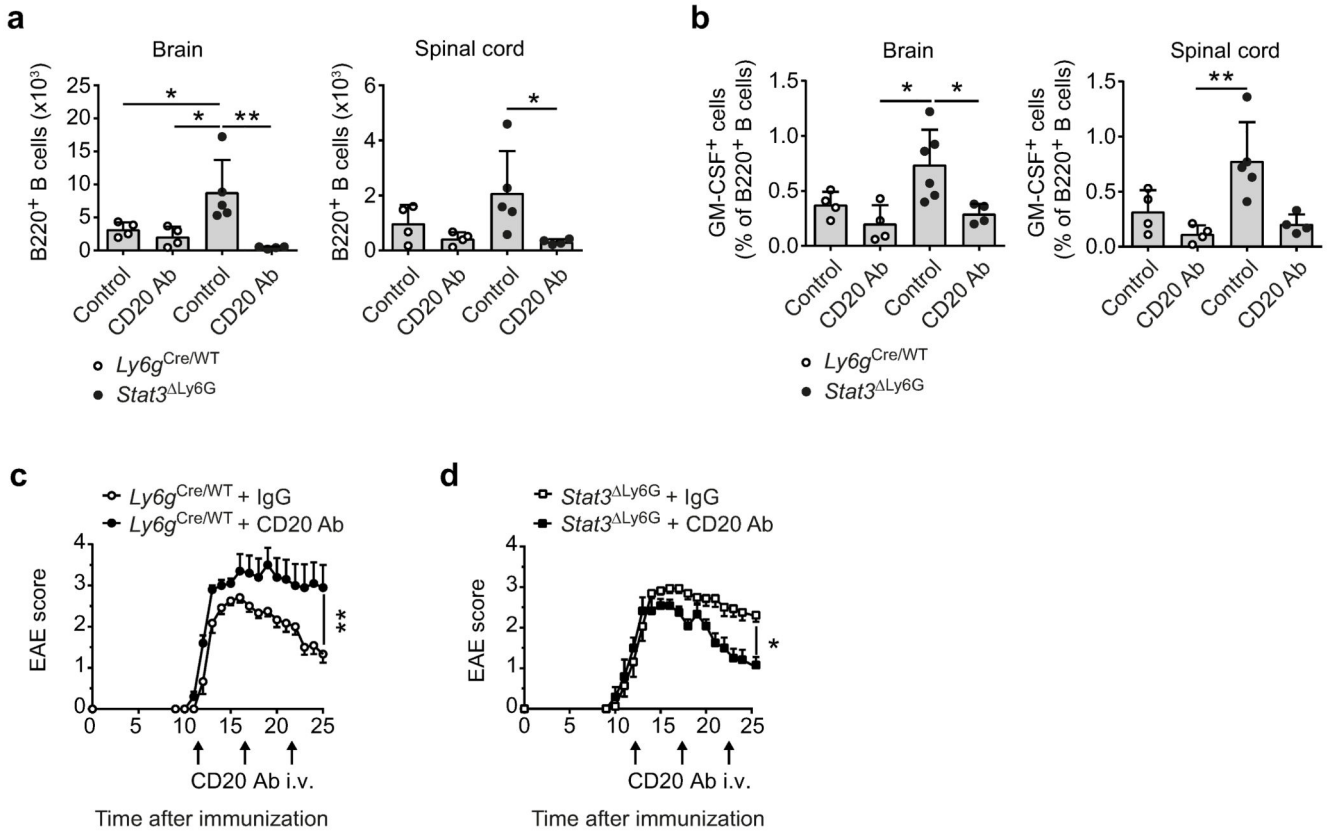

Figure 7. B cells determine disease progression in the absence of functional MDSCs.

a, b, Total numbers of $CD19^+B220^+$ B cells **(a)** and frequencies of GM-CSF-producing $CD19^+B220^+$ B cells **(b)** within the $CD45^+$ compartment in the brain and spinal cord of *Ly6g*$^{Cre/WT}$ and *Stat3*$^{\Delta Ly6G}$ mice at disease recovery (d25) when the mice were either control treated (IgG1κ) or i.v. injected with 10 μg/g CD20 antibody (CD20 Ab) every 5 days starting on day 12 after immunization; symbols depict individual mice (bars mean ± SD); Kruskal-Wallis-test with Dunn's post test; *p<0.05, **p<0.01. **c,** EAE disease course in *Ly6g*$^{Cre/WT}$ control mice treated with IgG1κ control antibody (n=4) or CD20 antibody (CD20 Ab, n=4); symbols depict means and s.d.; two-way ANOVA with Bonferroni's multiple comparison; **p<0.01. **d,** EAE disease course in *Stat3*$^{\Delta Ly6G}$ mice treated with IgG1κ control antibody (n=5) or CD20 antibody (CD20 Ab, n=4); symbols depict means and s.d.; two-way ANOVA with Bonferroni's multiple comparison; *p<0.05.

Europe PMC Funders Author Manuscripts